Load Flow Study for Utility-Scale Wind Farm Economic Operation and Reactive Power Grid Compliance

Christopher M. Moon

Thesis submitted to the Faculty of the Virginia
Polytechnic Institute and State University
in partial fulfillment of the requirements for the degree of

Master of Science
In
Electrical Engineering

Saifur Rahman, Chair
Virgilio A. Centeno
Jaime De La Reelopez

June 3rd, 2024
Blacksburg, Virginia

Keywords: Renewable energy, power systems, wind farm, newton-raphson, load flow, reactive power flow, active power loss

Load Flow Study for Utility-Scale Wind Farm Economic Operation and Reactive Power Grid Compliance

Christopher M. Moon

ABSTRACT

With environmental and policy pressure to move towards cleaner fuel sources, wind energy is a proven technology that can be successfully implemented at the utility-scale and provide clean energy to the grid. Wind energy consists of many distributed wind turbines that are paralleled and connected to inject power to one location on the transmission grid. There are real power losses and reactive power drops that must be taken into consideration for these projects for plant performance and compliance. The better the performance of each new and operating wind farm installed, the more efficiently the grid operates as well as the less greenhouse gases generated. This thesis will first review the creation of an Excel tool to perform a load flow study given inputs for a wind farm using Newton-Raphson algorithms. Next, the results of the load flow analysis will be compared to an actual operating wind farm located in Texas to review the accuracy of the scenarios. Finally, alternative design and operating states for the wind farm are proposed and cases are simulated to review the impact on wind farm energy generation and reactive power provided to the grid. Finally, preferred improvements for future design and operational considerations are provided along with future areas of research and development.

Load Flow Study for Utility-Scale Wind Farm Economic Operation and Reactive Power Grid Compliance

Christopher M. Moon

GENERAL AUDIENCE ABSTRACT

This thesis is focused on improvements for wind farm design and operation to help wind farms generate more clean power to the grid. The thesis involves the creation of an Excel tool which can be used to complete required grid studies for real and reactive power flows within the wind farm to the point of connection with the transmission system. This analysis helps inform the wind farm design and operation to be more effective and operate more efficiently. An operating wind farm in Texas is explained and depicted for an understanding of how utility-scale wind farms are set up. Additionally, a year of data from an operating wind farm is used to compare the Excel load flow tool to actual data and confirm it's accuracy. Alternate methods this plant could have been designed and operated are evaluated using the new tool and actual operating conditions from the plant for the year under analysis are performed to better understand and quantify possible improvements for wind farms. This thesis is less focused on the wind turbine generator (WTG) construction and operation of a single unit, but rather focused on the output from the WTG and the impact on an entire system containing many of these distributed generators and their operation to provide energy to the grid.

Dedication

I dedicate this thesis to the Virginia Tech faculty that supported my studies and my family that allowed me the time to pursue this endeavor.

Acknowledgements

First, I would like to start by expressing my gratitude toward Dr. Saifur Rahman for supporting me throughout the process and providing me with the time, space, and guidance to pursue graduate studies at Virginia Tech. I would also like to acknowledge my committee members Dr. Centeno and Dr. De La Ree for their time and support. Completing a master's program is a significant time commitment, especially when coupled with working in industry, and without a supportive institution such as Virginia Tech this would not be possible. Pursuing this degree has furthered my knowledge and skills as an electrical engineer in the industry.

I am grateful for colleagues and professors whom I have interacted with over the past decade of my work and academic career which have given me the knowledge and curiosity to continue to learn and explore innovative ideas.

Finally, I would like to thank my family who has supported me with love and encouragement to complete this thesis.

Table of Contents

List of Figures

List of Tables

List of Abbreviations

AC	Alternating Current
ACSR	Aluminum Conductor Steel Reinforced
AGC	Automatic Generation Control
AHJ	Authority Having Jurisdiction
AVR	Automatic Voltage Regulator
BOP	Balance of Plant
CAD	Computer Aided Design
DC	Direct Current
DETC	De-Energized Tap Changer
DFIG	Doubly Fed Induction Generator
ERCOT	Electric Reliability Council of Texas
FACTS	Flexible AC Transmission System
FERC	Federal Energy Regulatory Committee
HV	High Voltage
HVRT	High Voltage Ride Through
IEEE	Institute of Electrical and Electronics Engineers
IBR	Inverter Based Resource
IGBT	Insulated Gate Bipolar Transistor
IPP	Independent Power Producer
IRR	Intermittent Renewable Resource
ISO	Independent System Operator
LMP	Locational Marginal Price
LVRT	Low Voltage Ride Through
MPT	Main Power Transformer
MV	Medium Voltage
NEC	National Electric Code
NERC	North American Electric Reliability Council
OEM	Original Equipment Manufacturer
OLTC	On Load Tap Changer
POI	Point of Interconnection
PPA	Power Purchase Agreement
PPC	Power Plant Controller
PRC	Protection and Control
PTC	Production Tax Credit
REC	Renewable Energy Credit
RTO	Regional Transmission Operator
SCADA	Supervisory Control and Data Acquisition
SCED	Security Constrained Economic Dispatch
STATCOM	Static Synchronous Compensator

US	United States
TO	Transmission Owner
QSE	Qualified Scheduling Entity
WTG	Wind Turbine Generator

Chapter 1

1.0 Introduction

The electric transmission grid in the Unites States (US) has seen a large increase in renewable generators to the system over the past decade. The volume of renewable energy generators seeking to interconnect and operate on the transmission system is increasing significantly with a growth in requests up 40% year over year in 2022, with approximately 95% of this proposed capacity being solar, wind, or battery storage [61]. Construction and operation of large conventional units is slowing with environmental mandates and political action and in its place, renewables are gaining more and more access to transmission interconnection rights. Many states in the US have released bold objectives to become net neutral on carbon emissions and one of the major drivers to achieving this is the installation of utility-scale renewable energy generators. This trend is expected to continue given the current queues in the Unites States with more than 2,000GWs of generation and storage in interconnection queues at the end of 2022 [58]. Additionally, the recent FERC Order 2023 is expected to help this transition and speed up transmission owner's (TOs) process to move generator filings through the queue in a quicker manner [58].

The primary deployment of renewable energy over the past decade has been solar and wind generation given commercial viability and land use. This trend is expected to continue over the coming years with an uptick in utility scale battery storage, especially as the price of lithium-ion decreases in correlation to electric vehicle demand, to provide grid support and reliability [59]. Today, solar and wind generation facilities consist of inverter-based resources (IBRs) with insulated-gate bipolar transistors (IGBTs) used to convert power between direct current (DC) and alternating current (AC) so that it can be provided to the transmission system at the appropriate voltage and frequency. Transmission connected solar facilities are typically using central

inverters and transmission connected wind facilities are typically using Type 3 and Type 4 wind turbine generators (WTGs), with Type 5 WTGs in a research stage. Sizes of each of each individual IBR for a facility may range from 3-6 MW each with output voltages of the inverter/converter typically less than 1000V. The design of a renewable energy facility connected to the transmission system will typically consist of dozens of IBRs connected in parallel to inject power to one node on the transmission grid. This requires the use of cables/conductors to connect the IBRs togethers and substations to safely step the output of the IBRs up to the transmission system voltage.

An important consideration for wind facilities is they are intermittent renewable resources (IRRs), meaning that they require the presence of a natural resource (e.g. wind) to produce power which is not always available. This has an impact on the IBRs ability to provide grid support functions such as frequency and voltage support on demand. Given this, it is important for the renewable generator to have an accurate electrical model of their facility to provide to the independent system operators (ISOs) and regional transmission operators (RTOs) and the TO for operational and planning purposes for grid reliability. Also, ISOs/RTOs are using meteorological data to predict generation facility modeled output for an upcoming dispatch period and will use this in their Security Constrained Economic Dispatch (SCED) point [3].

For active power, the resources will generate based on availability and will be paid/pay the locational marginal price (LMP) for every MWh generated/consumed at its point of interconnection with the transmission system. A plant may be curtailed from SCED from the ISO/RTO based on transmission congestion and/or LMP being lower than offer price. Typically, renewable energy generators will offer negative prices into the market and still generate even when real-time LMPs are negative given they do not have a cost for fuel, they are paid Renewable Energy Credits (RECs) for delivered power, and many facilities have a production tax credit (PTC) where they are given tax credit for MWhs delivered in the first 10 years of the facilities operation. A renewable plant may also be curtailed if the frequency at the point of interconnection with the transmission system is too high (e.g. not enough system load). Lastly the plant may also

self-curtail itself from its operation center if maintenance is needed on equipment.

For reactive power, the IBR will use IBGTs to offset the voltage and current angles and control reactive power output from the facility. Renewable energy plants will operate to a local target voltage setpoint at the point of interconnection with the transmission system. Based on this target voltage the facility may implement a voltage droop or other control method to provide/absorb VARs from the transmission system to maintain the localized target voltage. If there is a voltage dip at the point of interconnection (POI) the renewable generator will be expected to ride through and provide VARs. If there is a voltage spike at the POI the renewable generator will be expected to ride through and absorb VARs. Connecting many paralleled IBRs within a facility often located miles from one another leads to an importance on system design and operational control to ensure the plant is meeting voltage control requirements at the POI while also respecting bus voltage limits of the facility and operating in an economic manner.

Renewable energy is an important piece of the puzzle to helping reduce carbon emissions and creating a sustainable power system. The standards and requirements for interconnecting renewable energy to the transmission system will continue to evolve and owner operators must continue to evolve with it. The cohesion of design modeling and operational data will be important for the renewable generators to continue to improve upon the economics of their operation as well as improving reliability services facilities can offer the grid. Wind farm design and operations come with many challenges and associated opportunities for optimization, some of which will be explored in detail in this thesis.

A typical wind farm power curve characteristic for a site will look similar to the below. [51]

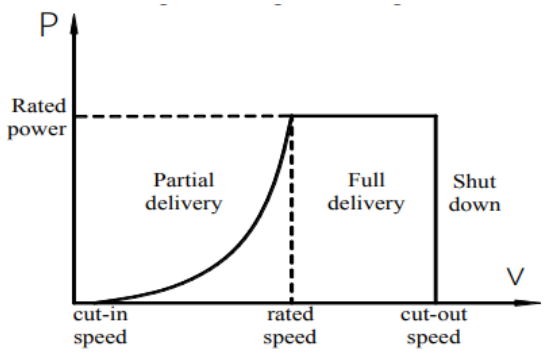

Fig. 1: Curve of power output-wind speed of DFIG

Source: Y. C. Chen, [51]

Figure 1.1 Typical Wind Farm Power Curve

Additionally, the variance in wind speed for a site will change many times throughout the day. A sample site wind speed with data taken from a met station every 10 mins is shown below in Figure 1.2 for perspective of how the power flow within the facility may vary over a day.

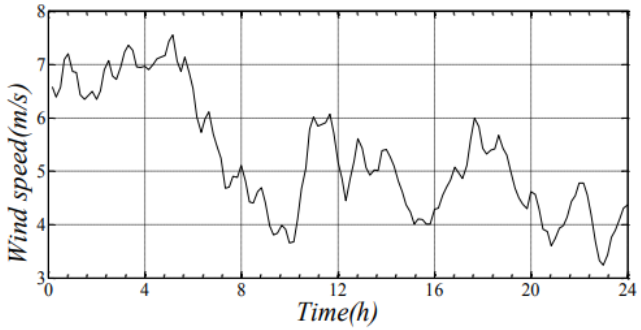

Fig. 2: One day wind speed curve

Source: Y. C. Chen, [51]

Figure 1.2 Typical Wind Farm Daily Load Profile

1.1 Motivation

The motivation for this thesis is two-fold. The first goal is the development of a power flow tool for a utility-scale wind farm to calculate balance of plant (BOP) active power loss and reactive power

drops within the facility. The second goal is using the power flow tool to assess design and operational considerations for the wind farm BOP to reduce active power energy loss while complying with the Federal Energy Regulatory Committee (FERC) Order 827 on reactive power control requirements for transmission—connected generators.

Traditional design methods for calculating estimated electrical energy loss for a generation facility would be to assume a generator power factor operating point, calculate out load currents, and then calculate load and no-load losses for the BOP equipment to the POI with the transmission system, where the revenue meter is located. Typically, an average operating power factor is assumed here because there is not a reliable mechanism for a wind farm independent power produced (IPP) to estimate out the TO voltage setpoint and changes in grid strength (short circuit MVA) to estimate required MVAr delivery/absorption on a discrete time interval into the future. A slightly lagging power factor is often assumed for the site average operating point based on historical induction generator operating points [62]. This thesis will create a model to model out the varying reactive and active power flow more accurately for a wind farm using conventional Newton-Raphson calculations and provide more insight into possible design and operational improvements to the facility.

An important distinction is this thesis will focus on technical losses as opposed to non-technical losses for power systems which is discussed in [45] and shown in a high-level diagram in Figure 1.3. Within technical losses there are fixed losses that do not vary by current flowing in the system and typically make up about one-fourth to one-third of the system losses [45]. Variable technical losses typically make up approximately two-thirds to three-fourths of the system losses [45]. This thesis will focus on reducing variable technical losses.

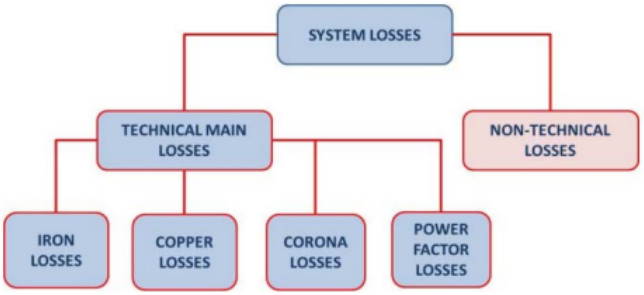

Source: C. Moldoveanu, [45]

Figure 1.3. Typical System Losses

Other losses not directly considered include harmonic losses, unbalanced load losses, and losses due to poor quality of equipment or degradation over time [45]. Non-technical losses include items such as inaccurate measurements, theft/fraud, error estimation losses, congestion losses, and incorrect use of measured data [45].

As noted above, the desire of this modeling effort is to reduce variable technical losses. In parallel to this, the wind farm must also comply with FERC 827 and provide +/-0.95 power factor capability at max MW output of the facility to the POI. To accomplish this the resistance, reactance and susceptance of equipment used in the wind farm BOP is important to understand. The most difficult scenario for the wind turbine induction generators occurs when they are operating in an overexcited state and providing VARs to the grid. This is due to the VAR drop across the BOP cables, transformers, and conductors making it more difficult to deliver the required reactive power to the POI.

To improve upon grid reliability to the project's POI, the project should be available to operate and provide primary frequency response and voltage support as the wind resource is available. Primary frequency response includes the generator controls active power output responding to grid frequency deviations per FERC Order 842. Additionally, wind farms are required to ride-through frequency and voltage deviations on the grid to provide reliability support. Ride-through for IBRs has proven to be difficult in many cases such as the Odessa Event in the Electrical

Reliability Council of Texas (ERCOT) on June 4th, 2022, where a fault occurred and was exacerbated by IBRs tripping offline when they should have ridden through the event per NERC standard PRC-024-3 and ERCOT nodal protocols leading to a wide-spread blackout [60]. Keeping generators online during transient conditions is important for grid stability and inherently IBRs do not have the same inertial response or reactive power injection as compared to conventional synchronous generators [63]. It is important to consider ride-through capability when looking at plant operation schemes to provide an appropriate response to grid conditions to help normalize the system quickly and avoid FERC penalties.

1.2 Objectives

The first primary objective of this thesis is to build a power flow study tool using the Newton-Raphson techniques for a utility-scale wind farm that will evaluate the site for FERC 827 compliance and provide electrical losses for the given operating state of the plant. The tool will take known state variables as inputs and provide a fully modeled state of the system. Historical supervisory control and data acquisition (SCADA) data is used for the site to analyze the tools relative accuracy.

The second objective of this thesis is to use the tool to assess other design and operational methods for the Texas wind farm and review the impact on site performance focused on an active power loss and reactive power flow standpoint. Future methods for design considerations and operational methods to improve the plant's performance are proposed.

1.3 Thesis Outline

First, the literature review will go through existing design and operational optimization techniques for wind farms. Next, the literature review will cover using Newton-Raphson load flow and annual energy assessment techniques commonly deployed both in the transmission and

distribution systems as well as some specifics for wind facilities.

Next, the Framework and Methodology section will cover the power flow model built in Excel and the comparison to SCADA data from an operating wind farm in Texas.

Finally, the Case Studies & Results section will cover different proposed design and operating modes for the wind farm and the subsequent results on power flow. The thesis will end with a conclusion of the results and recommendations for future work.

Chapter 2

2.0 Literature Review

This literature review will focus the first two sections on optimization considerations for design and operation of the wind farm BOP. The next two sections will focus on the steady-state analysis and electrical energy loss calculation considerations for plant performance. Finally, the last section will focus on some research gaps. This thesis is focused on wind farm BOP optimization and of note much of the research in the renewable energy industry is focused on hybrid renewable generation technologies, wind turbine generator design, or focused on the TO planning and operational side of renewable energy generator integration to the grid.

2.1 Optimized Wind Farm Design

Today's utility scale wind farms in the US are transmission connected (>69kV) and typically larger than 20MWs in capacity [64]. The WTGs are connected in parallel via daisy chain connections back to a substation where the voltage is stepped up from the commonly used 34.5kV collection system voltage to the transmission voltage of the local grid, which is typically in the range of 115kV to 765kV. Much of the electrical energy loss in a utility-scale wind farm is based on the 34.5kV network given the lower voltage and higher currents flowing through typically underground tree retardant, cross-linked polyethylene (TRXLPE) or ethylene propylene rubber (EPR) cables. Wind farm design has been researched over the past years with a focus on reducing capital and operational expenditure to arrive at a competitive power purchase agreement (PPA) price to compete with thermal generation. The focus of this literature review is around wind plant BOP design of which most of the discussion is applicable for solar plant design as well.

In the design of the wind farm, generally the WTG original equipment manufacturer (OEM) for

the site is chosen and then the wind turbines are sited across the project buildable area. Next, BOP equipment is specified to collect the power from each of the distributed WTGs to the transmission grid. Finally, a wind resource assessment is carried out to determine the expected annual energy generation of the facility to the grid.

Once the WTG locations are set based on the wind resource, the electrical design will determine how to connect the distributed resources back to the POI. This is typically accomplished via the collection system, substation, and transmission line. For the collection system, a decision tree is provided below in Figure 2.1 with varying objective functions, all of which can be solved with varying classical optimization techniques [21].

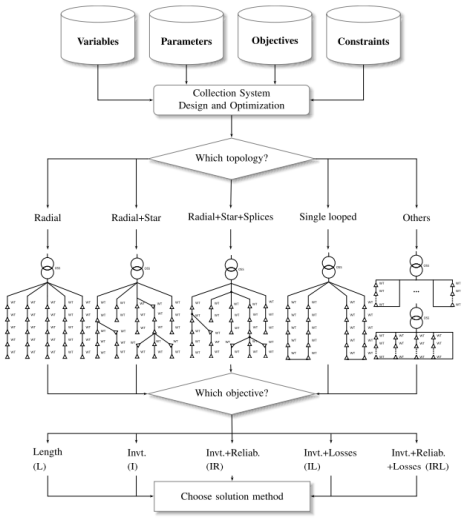

Source: J.-A. Perez-Rua, [21]

Figure 2.1 Collection System Objective Functions

The design engineer for the wind farm can choose the topology and the objective function to optimally locate facilities. Common design methods today include manually locating facilities in a computer aided design (CAD) software based on geographical constraints provided. However, the total investment in the 34.5kV collection system alone is estimated to make up 9%-27% of the total wind farm construction cost which is a large number that deserves attention [7]. Once an

objective function is chosen a solution method can be selected based on the below Figure 2.2 for optimizing collection system design and locating facilities [21].

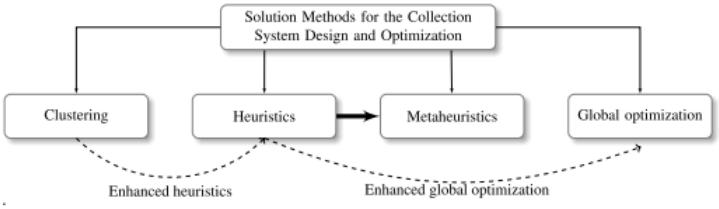

Source: J.-A. Perez-Rua, [21]

Figure 2.2 Collection System Optimization Techniques

Each section has different algorithms that can be deployed for optimization of facilities.
One approach is to use K Means clustering and Spectral clustering to automate IBR blocks in python to help automate the process and save engineering time to arrive at an optimized layout and groupings based on site topography and land constraints [5]. K Means clustering is commonly used for WTG placement based on the user set quantity of clusters as well [8]. Additionally fuzzy C-means clustering is another algorithm used to group the WTGs into different buckets [19]. The number of clusters will help drive the number of circuits back to the substation and will be driven by the cable ampacity and short circuit withstand of the cable or conductor used to connect the distributed IBRs.
For heuristics, minimum spanning tree (MST) is a commonly used algorithm for systematically determining the optimal loop-feed routing between wind turbines where the wind turbines are the nodes and the cables connecting them are the edges [8]. MST has two popular algorithms that are used including the Kruskal algorithm and the Prim algorithm [20]. This minimum spanning tree can be expressed at G_T with minimum total of W_T. See below formula for description.

$$G_T\,(V, E_T, W_T) \qquad G_T \in G, E_T \in E, W_T \in W$$

Figure 2.3 Minimum Spanning Tree Equations

Using an algorithm such as MST the typical wind farm WTG routing may look similar to Figure 2.4.

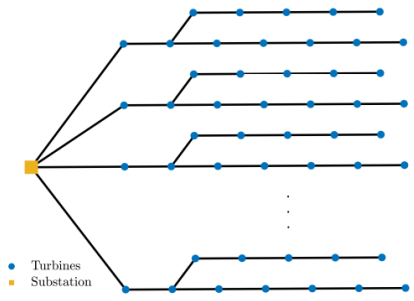

Source: C. E. Mokhi, [8]

Figure 2.4. Typical Wind Farm Collection System Routing

The genetic algorithm is another method deployed to minimize cable lengths and associated costs [14]. Mix integer linear programming (MILP) is an algorithm developed for cable cost minimization also considering electrical energy loss in [15] and [16]. The Ant Colony Optimization (ACO) is used in [17] to minimize cable losses and lengths. A modification of the Traveling Salesman Problem is used in [18] to determine optimal cable routing for a wind farm. Similar to other optimization problems, collection system routing can be completed optimally using many different algorithms. Another optimization technique used is the firefly optimization method which was developed by Yang [9] [10] [11] [12] and is used to optimize the shortest length routing between each of the WTGs in a cluster.

Clustering WTGs and applying an algorithm such as MST, GA or firefly supports finding the distance to minimize overall cable length while also seeking to minimize cable losses and minimizing relative capex given a set of inputs. However, the complexity in the real world is

working around landowner requirements and a very large dataset of cables, conductors, and other miscellaneous equipment, such as junction boxes, that may be used to support the system design. Similar to other optimization problems, collection system routing can be completed optimally using many different algorithms.

Another aspect of BOP wind farm design is the substation placement. The genetic algorithm is a method of locating the collector substation to have the sum of all the distances to all turbines minimized based on the evolutionary process [13]. Additionally, the Particle Swarm Optimization (PSO) is an optimization invented by Russel Eberhar in the US in 1995 [13]. The PSO starts with random initialized particles in the search area with each particle having a position and velocity. The theory to selecting the optimal position then is based on each particle's position influenced by it's own experience and also that of the other particles in each iteration [13]. An example of the GA and PSO algorithms can be seen below starting with the figure showing the initial wind farm layout in Figure 2.5 below.

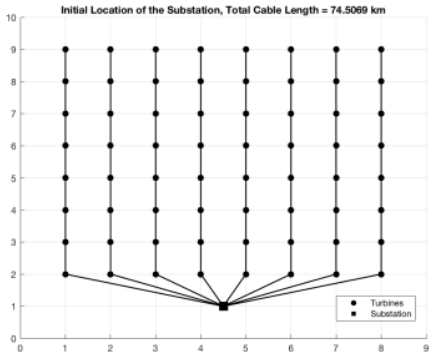

Source: C. E. Mokhi, [13]

Figure 2.5 Wind Farm Initial Substation Location

Then minimizing each function using the GA method results in the figure below.

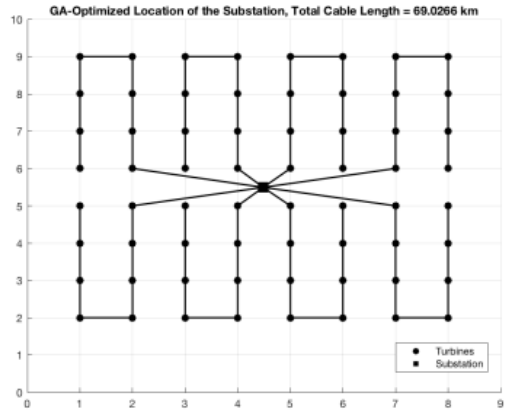

Source: C. E. Mokhi, [13]

Figure 2.6 Genetic Algorithm Optimization of Substation Location

The PSO algorithm also results in the same substation location as Figure 2.6. Figures 2.5 and 2.6 are general physical representations and ignore other placement considerations of the WTGs such as wake effect between the WTGs. Both optimizations result in a cable saving of 7.36% of the total wind farm cable system for this simple example [13]. The above optimization is a straightforward example, and the algorithms can be used for efficiencies in practice where array shapes are more irregular, and the optimal placement is much more difficult to visually determine.

Much of the recent research into wind farm design and optimization is focused on offshore wind but many of the concepts and algorithms use similar methods to those described in this section and are relevant for onshore applications as well. This section has covered the predominant design methods for BOP design for the wind farm centered around WTG collection system and substation placement. The next section will cover wind farm operation methodologies.

2.2 Optimized Wind Farm Operation

Wind farms operating in RTO/ISO markets in the US are required to follow NERC standards

which dictate minimum operating requirements, and the focus of this section will be on two of these – active power control and reactive power control. ERCOT also has requirements provided in their Nodal Protocols and Nodal Operating Guides with the same active and reactive power control requirements [65].

For active power control this includes AGC where the wind farm is bid into either the day ahead or real time market and, assuming the pricing cleared, the plant is dispatched in real time via SCED. In ERCOT, the generation facility is free to generate up to its maximum possible power if the entire site cleared in the market, which wind farms typically do with their low marginal cost per MWh, unless there is a curtailment, commonly due to low load or transmission congestion. ERCOT telemeters to each wind farm a base point (BP) and a SBBH (SCEC Base Point Below HDL) [65]. SBBH is a binary and when the binary is positive, the resource must begin to follow the site's BP due to system level constraints. The other active power control required by wind farms in the US is based on FERC 842 which requires primary frequency response performed by each generator owner, which is covered in NERC standard BAL-003-2 [22].

Wind farms will generate up to their maximum power available unless the AGC curtailment flag is issued by the RTO/ISO. Each WTG will operate in Q priority mode, such that it will maximize its active power generation subject to the required reactive power demanded of it from the power plant controller (PPC) to control POI voltage. Therefore, based on the wind resource each WTG will operate at the highest active power output it can based on its D curve/thermal limitations.

For reactive power control, this is accomplished through the automatic voltage regulator (AVR) which is a process by which the transmission owner sets a target voltage for the wind farm's POI and the wind farm will operate in a voltage control mode providing capacitive or inductive VARs to the grid as required to maintain the line voltage. The requirements and acceptable deviations for following the voltage targets as set by the transmission owner are prescribed by NERC in standard VAR-002-4.1 [23].

The PPC will control the reactive power by receiving a voltage setpoint from the transmission operator, converting this to a Q-target, and then dispatching available WTGs to meet this Q-

target. This can be accomplished in many different methods. A variable voltage-droop is a common method PPCs will deploy to determine the required VARs [26]. An adaptive Q-V scheme was also proposed in [27]. In [38] they propose an AVR strategy to use wind power prediction data and pre-switch capacitor banks. In [39] they use the optimal power flow mathematical problem to solve an objective function using equality and inequality constraints. Regardless of the voltage control algorithm selected for the PPC, it will need to respect the D curve of each WTG independently and available power from the wind to determine a dispatch point for the WTG [28]. When the voltage on the grid requires a reactive power setpoint change from the WTGs the plant must respond to maintain the grid voltage target performance per NERC standards.

For a utility-scale wind farm, typically the PPC is deployed to ensure AGC and AVR are dispatching the grid following IBRs to meet grid code compliance and there are different control architectures that PPCs deploy to do this [24]. For type-3 doubly fed induction generators, active and reactive power controls can be de-coupled for more precise control given the back-to-back converters [29]. The wind turbine PPC will also often include controls for damping oscillations, low and high voltage ride through, short circuit injection, and other transient phenomena. Additionally, utility-scale wind farms are required to have a dynamic system model, typically PSSE or PSCAD software models, to represent the site controls for interconnection studies by the transmission owner [25].

2.3 Steady-State Assessment

The steady-state assessment of a wind farm for performance focuses on limiting both active power loss and reactive power drop and methods of doing this in a reliable, safe, cost-effective manner. Due to the intermittent nature of WTGs, the active and reactive power available and provided to the grid will vary and it is important to evaluate the different possible scenarios to best understand the operating points of the plant. NERC requires a facility to be able to operate to at least a 0.95 leading and lagging power factor at the POI and an electrical load flow study and

testing is required to verify this capability [30]. There are many different algorithms and computer programs to complete this assessment.

When performing a load flow, the first step is to create a system representation, most commonly done by placing the plant data into a per unit model. The system representation will consist of bus data, generator data, branch data, and transformer data [31]. The first load flow solution device was a computer called an AC network analyzer built around the late 1920's [31]. As computers emerged in the late 1950's and algorithms could be solved in a more efficient manner, Wade and Hale developed the first load flow program using a modified Newton iterative process in 1956 [32]. Soon after this followed the Gauss-Siedel algorithm development. Developments in load flow algorithms continued and in the early 1960's the Newton-Raphson iterative method was developed and is still at the core of many load flow computer programs today [33].

Load flow of a wind farm can be performed with Newton-Raphson and it can be setup using the standard PV, PQ, and swing bus setup. Each WTG can be modeled as a PQ generator bus operating in the opposite direction from a PQ load bus [34]. Next the nacelle transformers and the substation transformers can be converted to per unit with the same bases. For nacelle transformers, these typically include de-energized tap changers (DETCs), which can be modeled at a fixed tap. However, most wind farms use OLTC's on their large substation main power transformers (MPTs) to support voltage drop across the long collection cable runs to keep WTGs far way from the substation within an acceptable operating voltage range. The substation MPT's with their high voltage (HV) OLTCs are modeled as shown in [34]. This model accurately takes the tap position and its effect on the transformer impedances into account for modeling.

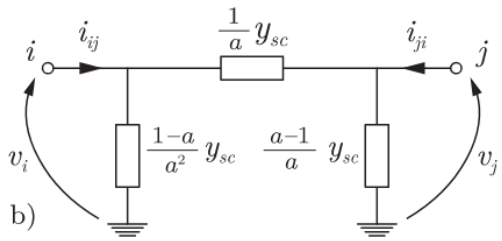

π equivalent traditional models of tap-changing transformers

Source: J. D. Glover, [34]

Figure 2.7 Pi Model of a Transformer with a OLTC

Shunt capacitor banks and reactor banks are commonly used in wind farm project substations for reactive power support and can be modeled as PQ busses as well when performing Newton-Raphson load flow for a wind farm. The POI is modeled as a swing bus. With this the entire wind farm can be modeled using the Newton-Raphson techniques.

Much of the research into modeling of wind farms is focused on aggregation of the wind farm as a single resource for steady-state transmission system analysis and transient phenomena such as harmonics and sub-synchronous oscillations and the associated modeling.

2.4 Annual Energy Loss Modeling

The two main sources of loss in a wind farm are the WTG (including mechanical losses, energy conversion losses, and losses in transformers) and the collection system, including BOP equipment [37]. The desire is to minimize annual electrical energy loss considering the design and operational aspects of the wind farm. First, we define electrical energy loss for a wind project as the technical losses from the output of the wind turbine terminal to the grid POI.

Minimizing the annual energy loss for a wind farm will also decrease the voltage drop across collection system and BOP components and increase reliability provided to the grid [40]. As the size of the wind farm increases the collection system lines become longer and number of circuits is higher and voltage deviations and active power loss are a larger concern [37]. To reduce annual

energy loss, there has been research in [37] to use the objective function to minimize voltage deviations on the collection system and minimize the system losses considering the constraints of active and reactive power flow at each node [37]. When determining active and reactive power losses for a wind farm or any electrical power system, the below basic equations can be used which use an equivalent resistance method [40] [46]. These form the basis for the losses of the system, primarily heat losses.

$$P_L^t = \sum_{i=1}^{N_{line}} \left\{ (I_i^t)^2 \times R_i \right\}$$
$$Q_L^t = \sum_{i=1}^{N_{line}} \left\{ (I_i^t)^2 \times X_i \right\}$$

Source: M. Purlu, [40]

Figure 2.8 Basic Active Power Loss and Reactive Power Drop Equations

Additionally, there are transformer losses, both load loss and no-load loss, present in the BOP annual electrical energy loss. Another method for determining the losses of a system is by performing power flow using Newton Raphson [46] which is especially helpful when analyzing a complex system where the currents may not be easily known given capacitive reactance and network topology [46].

There has been research into minimizing electrical losses for more efficient operation both on the transmission/distribution power system side as well as the IBR plant side. Strategies on the power grid side have included methods such as active load sharing, VAR injection and transformer tap changing [41]. Active load sharing is accomplished by providing generation to loads via the power system network to minimize line current and associated losses [41]. VAR injection focuses on prioritizing reactive power injection at the lower per unit voltage busses as opposed to the higher per unit bus voltages [41]. Changing the transformer tap positions is a strategy where optimal power flow is completed, and varying tap positions are reviewed to determine the position with the lowest electrical energy loss across the system [41]. For the grid with a very large number of nodes, the electrical energy loss is sometimes also calculated using algorithms such as the cluster analysis, neural networks, regression algorithms and support

vector machine algorithms to cut down on computing time [46]. Equivalence resistance and forward-backward sweep methods are also commonly deployed on the distribution system and using these methods the system operators can determine the optimal operating point based on predicted energy demand into the future [50]. On the distribution operations side, in [54] they use modified particle swarm optimization to reconfigure the distribution system in real time to the solving for the minimal active power loss scenario. Increasing the voltage on the distribution network is another loss minimization effort shown in [55] using a voltage booster to increase the system voltage by 50% and reduced system losses by approximately 5%.

Additionally, power system level loss analysis research has also been focused on minimizing grid losses by the addition and dispatch of wind farms as shown in [49] [52]. Given the market operations and wind farms having a low marginal operating cost, wind farms are often generating in real time over other conventional systems which makes minimizing transmission system losses more complex for the grid operators.

Wind farm BOP electrical energy loss minimization has also been researched. In [42] they review the site level Q dispatch and select individual WTGs to provide associated VARs to minimize active power loss based on static wind farm parameters (e.g. wind farms closer to the substation as available). In [43] an equal power factor algorithm was used for assigning Q commands to individual WTGs. In [44] they focused on minimizing the amount of reactive power injected from the WTGs to minimize current and associated losses in the system using static var generators. [44] used the below objective functions, along with power flow equations, and constraints as a proposed method to minimize wind farm losses.

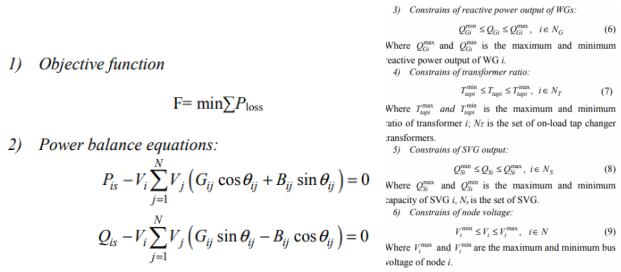

1) *Objective function*

$$F = \min \sum P_{loss}$$

2) *Power balance equations:*

$$P_{is} - V_i \sum_{j=1}^{N} V_j \left(G_{ij} \cos\theta_{ij} + B_{ij} \sin\theta_{ij} \right) = 0$$

$$Q_{is} - V_i \sum_{j=1}^{N} V_j \left(G_{ij} \sin\theta_{ij} - B_{ij} \cos\theta_{ij} \right) = 0$$

3) *Constrains of reactive power output of WGs:*

$$Q_{Gi}^{min} \le Q_{Gi} \le Q_{Gi}^{max}, \quad i \in N_G \qquad (6)$$

Where Q_{Gi}^{min} and Q_{Gi}^{min} is the maximum and minimum reactive power output of WG i.

4) *Constrains of transformer ratio:*

$$T_{tapi}^{min} \le T_{tapi} \le T_{tapi}^{max}, \quad i \in N_T \qquad (7)$$

Where T_{tapi}^{max} *and* T_{tapi}^{min} is the maximum and minimum ratio of transformer i; N_T is the set of on-load tap changer transformers.

5) *Constrains of SVG output:*

$$Q_{Si}^{min} \le Q_{Si} \le Q_{Si}^{max}, \quad i \in N_S \qquad (8)$$

Where Q_{Si}^{min} and Q_{Si}^{min} is the maximum and minimum capacity of SVG i, N_s is the set of SVG.

6) *Constrains of node voltage:*

$$V_i^{min} \le V_i \le V_i^{max}, \quad i \in N \qquad (9)$$

Where V_i^{max} and V_i^{min} are the maximum and minimum bus voltage of node i.

Figure 2.9 Active Power Loss Optimization Objective Function and Constraints

One of the issues with [44] is that this algorithm requires a large computer power to process and requires the control system to have access to transformer tap positions and real time voltage limitations, which is not often the case. To simplify power loss calculations, [47] proposed an apparent power-loss based method for aggregating the collection system to determine the active power losses of a wind farm. A method for aggregating the WTGs, WTG step-up transformer and collection system together to simplify loss estimation is discussed in [48] in which their simplified model can closely estimate the losses compared to the detailed model [48]. However, there is less room with a simplified model to evaluate loss performance improvement metrics. In [53] electrical loss performance estimation shows reduced losses from installing the static synchronous compensator (STATCOM) and recommends the use of Flexible AC Transmission System (FACTS) devices for minimizing electrical energy loss. However, these devices are expensive and can be complex to integrate into the wind farm. [53] also discusses the importance of operational settings (e.g. which devices are allocated first through last for reactive compensation) on overall loss performance.

There is also much research into the losses of the individual WTGs. Wind farms typically have an availability around 98% and a net capacity factor of 35-45% [56]. In [56] [57] the focus is on minimizing losses in the individual wind turbine generator, converter, and gear box when considering the wind distribution in a Weibull distribution to support the optimal design of the WTG. While many of the same equations can be used to minimize internal electrical energy losses of the WTGs, the focus of this thesis is on the BOP electrical energy losses.

2.1 Research Gaps

Significant work has been undertaken in the field of optimization for wind farm design, including the substation location placement and the routing of the collection system. However, much of this research uses classical optimization techniques and becomes very complex when trying to capture

specific items such as real-world constraints from landowners, land topology, and varying types of cables, conductors, and equipment. The optimization problem becomes very difficult to define economic constraints in meaningful terms.

Evaluation into the field of meeting active and reactive power injection requirements to the grid has received research wind farms. Plant controllers have varying control techniques, and these have been explored with many of the algorithms having merits. Additionally, research has shown some of the benefits of adding reactive compensation devices to the BOP system and the benefits. However, there is a gap in the BOP operation as it is typically viewed as a static impedance part of the plant controls. The optimization of design and operation of the wind farm at a plant level outside of the wind turbine itself is a gap and a focus of this thesis.

Additionally, much research has been conducted on the methods of modeling power flow for determining electrical energy loss with varying techniques for cutting down on computation time. Typical power flow equations are used in much of the research. However, using the power flow results to make decisions for design and operation of a wind farm is not commonly researched and can have a material impact on the plant performance. This thesis will focus on the method for assessing the power flow of a wind farm and using this data to review plant performance for varying design and operating conditions.

Chapter 3

3.0 Framework & Methodology

This chapter will start with a discussion on Newton-Raphson calculations for performing a load flow study. Next this chapter will review how the non-linear equations in Newton-Raphson load-flow were linearized to develop a wind farm model in Excel. Finally, the chapter will review the accuracy of the model data to the real-world data from the wind farm.

3.1 Load Flow

3.1.1 Power System Equations

This section will cover the setup of the power system equations and solving them using Newton-Raphson equations. First, the definition for apparent power at any bus in the network is defined by the below equation with subscript "i" designating the from bus and "j" designating the to bus.

$$\bar{S}_i = \bar{V}_i \, \bar{I}_i^* = \bar{V}_i \sum_{j=1}^{n} (\bar{Y}_{ij} \, \bar{V}_j)^* = P_i + j \, Q_i \tag{1}$$

The above equation can be further broken down to define active and reactive power flows at each bus in the system splitting out the admittance into conductance and susceptance and breaking down the phasor annotation with cosine and sine functions of the voltage angle between each bus as shown in equations (2) and (3).

$$P_i = \sum_{j=1}^{n} [\, V_i \, V_j \, G_{ij} \cos(\partial_i - \partial_j) + V_i \, V_j B_{ij} \sin(\partial_i - \partial_j)] \tag{2}$$

$$Q_i = \sum_{j=1}^{n} [\, V_i \, V_j \, G_{ij} \sin(\partial_i - \partial_j) - V_i \, V_j B_{ij} \cos(\partial_i - \partial_j)] \tag{3}$$

The next topic to cover in load flow is the setup of the admittance matrix, also referred to as a Y bus. The Y bus is a symmetrical matrix containing the admittances between each of the nodes and the self-admittance of each node. The rows and columns of the Y bus matrix correlate to the bus numbers in the system the Y bus is representing. Shown in Figure 3.1 below is the matrix equation of the Y bus and how it is used to correlate voltages and currents between buses. The Y bus is built per the following two requirements [66]:

(1) Off diagonal elements are the -1 multiplied by the admittance between the bus number of the column and the bus number of the row.

(2) Diagonal elements of the Y bus are the sub of all the admittances connected to the row/column number.

Figure 3.1 also provides an example of how a Y bus is constructed for a 3-node system with y_{ij} representing the admittance between bus i and bus j in the network.

$$\begin{bmatrix} \overline{I_1} \\ \cdot \\ \cdot \\ I_n \end{bmatrix} = \begin{bmatrix} \\ \overline{Y_{bus}} \\ \\ \end{bmatrix} \begin{bmatrix} \overline{V_1} \\ \cdot \\ \cdot \\ \overline{V_n} \end{bmatrix} \qquad Y = \begin{pmatrix} y_1 + y_{12} + y_{13} & -y_{12} & -y_{13} \\ -y_{12} & y_2 + y_{12} + y_{23} & -y_{23} \\ -y_{13} & -y_{23} & y_3 + y_{13} + y_{23} \end{pmatrix}$$

Figure 3.1 Y bus Matrix Example

3.1.2 Power System Bus Definition

In the above section, the power flow equations and Y bus matrix were covered. Next, for an electrical system there are 3 types of buses depending on the electrical equipment operating at the respective node. The 3 types of nodes are listed in Figure 3.2 below along with the known and unknown variables for this type of bus definition. Subscript "i" designates the respective bus

number.

Specified Quantities		Unknown Variables
Load bus	P_i, Q_i	V_i, θ_i
Gen bus	P_i, V_i	Q_i, θ_i
Slack bus	V_i, θ_i	P_i, Q_i

Figure 3.2 Electrical Busses and Variables

In a load flow analysis, there can only be one slack bus where the voltage magnitude and angle are fixed [31]. For renewable energy facilities connected to the transmission system the swing bus is located at the POI due to the relative grid strength of the transmission system compared to the generation facility. For each bus type there are 2 known and 2 unknown variables. The next section will cover the use of Newton-Raphson to solve for the unknown variables.

3.1.3 Newton-Raphson Method

The Newton Raphson method is an industry standard method to solve roots of non-linear equations [1]. The method considers a non-linear set of algebraic equations –

$$f_i(x_1, x_2, x_3, \dots, x_n) = 0;\ i = 1, 2, 3, \dots, n \tag{4}$$

The first step is to take an initial guess at the solutions to the unknown variables. The function f(x) for a single variable can be expanded using Taylor series expansion to result in the below equation [4]. x^0 is the initial guess and Δx^0 is the deviation from the root solution.

$$f\left(x^{[0]} + \Delta x^{[0]}\right) = f\left(x^{[0]}\right) + f'\left(x^{[0]}\right)\Delta x^{[0]} + \frac{1}{2!} f''\left(x^{[0]}\right)\Delta x^{[0]^2} + \frac{1}{3!} f'''\left(x^{[0]}\right)\Delta x^{[0]^3} + \dots = c \tag{5}$$

Assuming Δx^0 is small, higher order terms can be neglected and the equation can be approximated based on the first two terms as provided in (6).

$$f\left(x^{[0]} + \Delta x^{[0]}\right) \approx f\left(x^{[0]}\right) + f'\left(x^{[0]}\right)\Delta x^{[0]} = c \tag{6}$$

Starting with x^0 the correct solution can be iteratively calculated with the following.

$$\Delta x^{[0]} = \frac{c - f\left(x^{[0]}\right)}{f'(x^{[0]})} = \frac{\Delta f\left(x^{[0]}\right)}{f'(x^{[0]})} \tag{7}$$

Then the improved iterative solution for the variable can be directly calculated from

$$x^{[1]} = x^{[0]} + \Delta x^{[0]} \tag{8}$$

The process continues until the deviation between the calculated and the previous value are within acceptable limits.

$$\Delta f^{[k]} \leq \varepsilon \tag{9}$$

Each iteration of improves on the initial guess and the error between each iteration should decrease. Some important limitations to the Newton-Raphson method include requirements for the function to be smooth and continuous [2]. Additionally, the solution may not exist and even if it does, it may not be unique.

3.1.4 Newton-Raphson Power Flow

The above sections 3.1.1 through 3.1.3 provide background on the equations, bus types, and computation method required to use the Newton-Raphson method to solve power flow problems. Now to solve the power flow we are seeking to define the $|V|_i$, δ_i, P_i, and Q_i at each node on the system. The equations are typically set up and solved in per unit to simplify calculations.
First, we define all buses in the system as either PQ or PV buses, with a single slack bus. For the wind farm model, the POI is the swing bus and every other bus in the system including the generator buses can be treated as PQ buses for assessment of load flow and electrical losses. Active and reactive power equations can be calculated at each node in the system for the initial operating state (P_i, Q_i) and for the next iterative active and reactive power equations with the initial voltage magnitude and phase angle used ($P_i(x^0)$, $Q_i(x^0)$). This is shown in matrix form in

equation 10.

$$\begin{bmatrix}\Delta P_i \\ \Delta Q_i\end{bmatrix} = \begin{bmatrix}P_i \\ Q_i\end{bmatrix} - \begin{bmatrix}P_i(x^0) \\ Q_i(x^0)\end{bmatrix} \tag{10}$$

Power flow has multiple variables and the derivative of the function in the NR equations is now replaced with a partial derivative matrix, called the Jacobian Matrix.

$$f' = \begin{bmatrix}\frac{\partial P_i}{\partial \delta_i} & \frac{\partial P_i}{\partial |V_i|} \\ \frac{\partial Q_i}{\partial \delta_i} & \frac{\partial Q_i}{\partial |V_i|}\end{bmatrix} = \begin{bmatrix}\mathrm{J}_{P\delta} & \mathrm{J}_{P|\mathrm{V}|} \\ \mathrm{J}_{Q\delta} & \mathrm{J}_{Q|\mathrm{V}|}\end{bmatrix} \tag{11}$$

The equation below can then be used to form the solution to the Newton Raphson load flow.

$$\begin{bmatrix}\Delta P_i^{[k]} \\ \Delta Q_i^{[k]}\end{bmatrix} = \begin{bmatrix}\frac{\partial P_i}{\partial \delta_i}^{[k]} & \frac{\partial P_i}{\partial |V_i|}^{[k]} \\ \frac{\partial Q_i}{\partial \delta_i}^{[k]} & \frac{\partial Q_i}{\partial |V_i|}^{[k]}\end{bmatrix} \begin{bmatrix}\Delta \delta^{[k]} \\ \Delta |\mathrm{V}|^{[k]}\end{bmatrix} \tag{12}$$

Taking the inverse of the Jacobian Matrix sets up the equation to solve for the change in voltage magnitudes and phase angles between iterations.

$$\begin{bmatrix}\Delta \delta^{[k]} \\ \Delta |\mathrm{V}|^{[k]}\end{bmatrix} = \begin{bmatrix}\mathrm{J}_{P\delta}{}^{[k]} & \mathrm{J}_{P|\mathrm{V}|}{}^{[k]} \\ \mathrm{J}_{Q\delta}{}^{[k]} & \mathrm{J}_{P|\mathrm{V}|}{}^{[k]}\end{bmatrix}^{-1} \begin{bmatrix}\Delta P_i^{[k]} \\ \Delta Q_i^{[k]}\end{bmatrix} \tag{13}$$

With the change in the variables for the respective iteration, the next iteration of the voltage phase angle and magnitude can now be calculated per equation (14) by adding the change to the previous iteration value.

$$\begin{bmatrix} \delta_i{}^{[k]} \\ |V_i|^{[k]} \end{bmatrix} = \begin{bmatrix} \delta_i{}^{[k-1]} \\ |V_i|^{[k-1]} \end{bmatrix} + \begin{bmatrix} \Delta\delta_i{}^{[k]} \\ \Delta|V|_i{}^{[k]} \end{bmatrix} \quad (14)$$

This iterative process in the Newton-Raphson algorithm is continued until the error between the calculated quantities is within a given tolerance.

$$\begin{bmatrix} \Delta P_i^{[k]} \\ \Delta Q_i^{[k]} \end{bmatrix} \leq \varepsilon \quad (15)$$

3.2 Texas Wind Farm Model Development

As seen from above sections using the Newton-Raphson calculations can be used to solve for unknown variables on the power system given known variable inputs and approximating other values until they converge on a solution. A utility-scale wind facility will typically have a couple hundred buses, so for practical purposes a computer-based tool is used for modeling. This section will first provide a description of an operating Texas wind farm that the Excel model was built around. Next a dive into the Excel model development will be provided including how it was built, how it works, and how the non-linearity of Newton-Raphson equations are formulaically linearized for a program such as Excel to perform the calculations.

3.2.1 Texas Wind Farm

The Texas wind farm is an operating wind farm that is used as a typical reference site for this thesis. The site uses Siemens Gamesa 3.465MW rated WTGs. These are type 3 machines and have rectangular D curve capability. There are a total of 47 WTGs at the site for a rated wind farm capacity of 162.855MW. The Texas wind farm was built and commissioned in 2019. The output of each WTG is a pad-mounted transformer which steps up the turbine output voltage from 690V to 34.5kV. From the 34.5kV output of each WTG, nearby turbines are connected in

parallel via underground XLPE aluminum cables via loop feed connections. The largest cable size used is 1250kcmil aluminum and the ampacity of this cable can support up to approximately 7 of these WTGs. The site consists of 7, 34.5kV collection feeder circuits that collect the generation back to the project substation. Each feeder is connected to a circuit breaker at the project substation and then to a single 34.5kV medium voltage (MV) bus at the collector substation. Also connected to the 34.5kV MV bus at the substation are 3 separate capacitor banks, each rated for 13.5MVAr at 34.5kV. The substation includes a single main power transformer at the project substation which goes from 34.5kV MV bus voltage to 138kV transmission voltage and has an ONAF2 rating of 184MVA. The 138kV high voltage bus has a direct connection to the TO switchyard via 795 ACSR conductors. A simplified diagram of the facility is included in the diagram below.

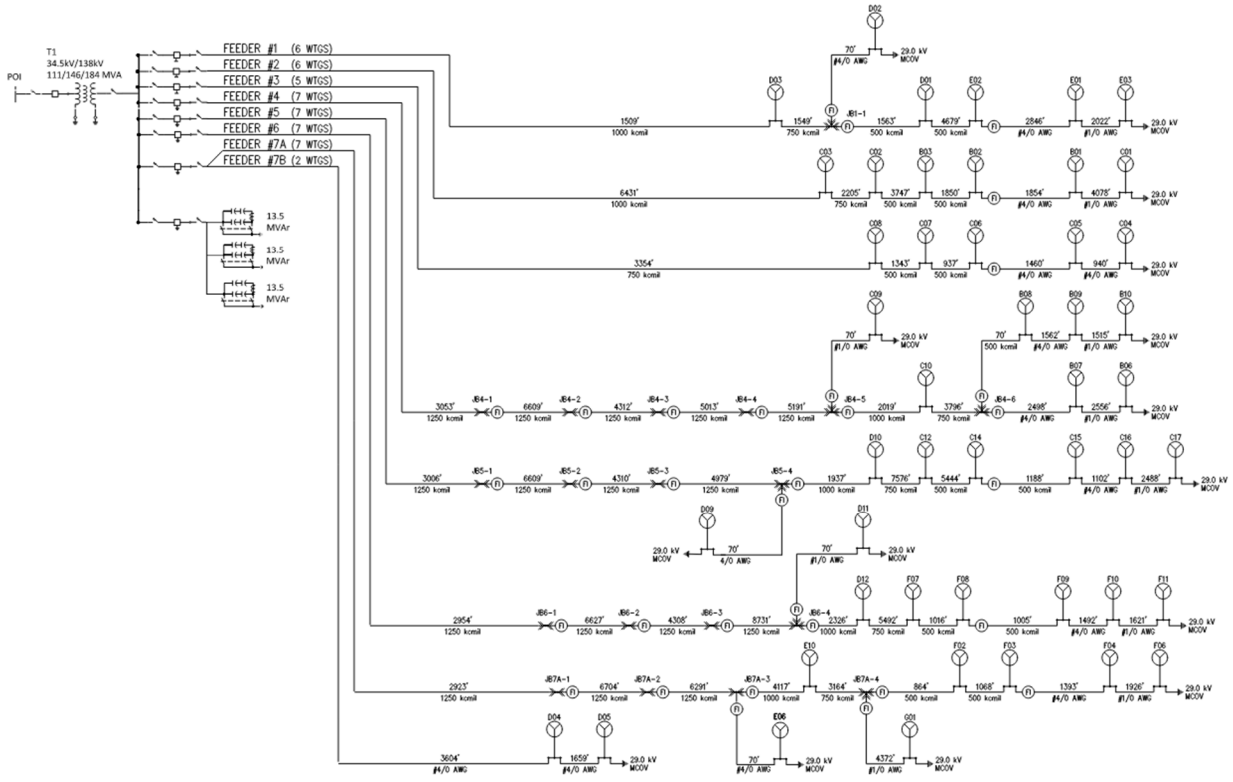

Figure 3.3 Simplified Texas Wind Farm Single Line Diagram

This Texas wind farm represents a typical wind farm design and was selected to help verify the accuracy of the Excel model build for this thesis when compared to site SCADA data. The next section will cover the setup of the Excel model to perform a load flow analysis on the plant outputs and grid conditions.

3.2.2 Excel Model Development

This section will take a deeper dive into the Excel tool developed to perform the Newton-Raphson load flow for the Texas wind farm. The primary focus of the Excel tool is to provide the voltage magnitudes and phase angles of each bus so power flows can be calculated and total electrical energy losses and reactive power drop for the system can be calculated. The Excel spreadsheet is broken out into 7 separate tabs as seen in Figure 3.4. The only tabs requiring user input are the Overview tab and the Impedance tab. All other tabs compute automatically to complete the required Newton-Raphson equations and outputs results on the Overview tab. Below each of the following figures will be a description of the formulas and calculations included in the respective tab of the Excel tool.

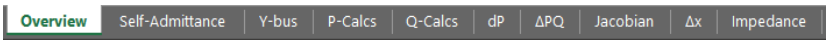

Figure 3.4 Overview Section

The Overview section can be broken down into two subsections. The first subsection includes the input data section. This section is used to list all electrical connections in the system from the WTG LV bus to the POI including cable, transformer, and junction box connections. All cells in green are manual inputs based on the project specifics and grey cells are the column/row descriptor. "Percent Wind Farm MW Output" and "Percent Wind Farm MVAr Output" allow the user to select the nameplate output percentage of active and reactive power at the WTG level across the site. The tool will then calculate out "Source MW" and "Source MVAr" in columns B

and C in per unit, respectively. The "LTC Position" refers to the substation main power transformer. It is an on-load tap changer (OLTC), which can move tap positions while the unit is energized and is located on the high side of the substation main power transformer, regulating the MV bus voltage to 34.5kV +/- 2%. This tap position is manually selected to regulate the MV bus voltage in the tool. The "From Bus", "From Bus (No.)" and "To Bus" are all populated based on the layout of the wind farm connections with the associated "cable/equipment type" and "Distance (ft)". The user selects the "Cable/Equipment Type" in the tool, along with a "Distance (ft)" distance if a cable/conductor is selected, and the tool will look-up the impedance data from the "Impedance" sheet.

The "PI Model Impedance" is all auto-populated based on the selected "Cable/Equipment Type" and "Distance (ft)" and pulling the respective data from the "Impedance" tab. The conductance and susceptance are calculated for each cable/transformer as well. There is a small amount of conductance and susceptance noted for the WTG transformers with off-nominal taps.

Subsection 1 - Inputs

	A	B	C	D	E	F	G	H	I	J	K	L	M	N	O	P
1		Percent Wind Farm MW Output	100%													NR Iteration / NR Reset
2		Percent Wind Farm MVAr Output	100%	LTC Position	16					PI Model Impedance						
3		Base MVA =	100	LTC Multiplier (a)	1.1					From Bus Z		From Bus Shunt Y		To Bus Shunt Y		
4		From Source MW (pu)	From Source MVAr (pu)	From Bus	From Bus (No.)	To Bus	To Bus (No.)	Cable/equipment type	Distance (ft)	+R (per unit)	+X (per unit)	+G (per unit)	+B (per unit)	+G (per unit)	+B (per unit)	Admittance 1/(R+jX) (per unit)
5	Feeder #1	0.03465	0.01423	E03-LV	1	E03-MV	7	transformer	transformer	0.27001	2.70080	0.00079008	-0.00790	-0.00077081	0.00771	0.036650026586267 8-0.3665972236049 7i
6		0.03465	0.01423	E01-LV	2	E01-MV	8	transformer	transformer	0.29077	2.90846	0	0.00000	0	0.00000	0.034033193098201 4-0.3404219658843 9i
7		0.03465	0.01423	E02-LV	3	E02-MV	9	transformer	transformer	0.27001	2.70080	0.00079008	-0.00790	-0.00077081	0.00771	0.036650026586267 8-0.3665972236049 7i
8		0.03465	0.01423	D01-LV	4	D01-MV	10	transformer	transformer	0.29077	2.90846	0	0.00000	0	0.00000	0.034033193098201 4-0.3404219658843 9i
9		0.03465	0.01423	D02-LV	5	D02-MV	11	transformer	transformer	0.27001	2.70080	0.00079008	-0.00790	-0.00077081	0.00771	0.036650026586267 8-0.3665972236049 7i
10		0.03465	0.01423	D03-LV	6	D03-MV	13	transformer	transformer	0.27001	2.70080	0.00079008	-0.00790	-0.00077081	0.00771	0.036650026586267 8-0.3665972236049 7i
11		0	0	E03-MV	7	E01-MV	8	1/0 AWG	2022	0.04043	0.00917	0.00000	0.00018	0.00000	0.00018	23.522949563973 7-5.337309708483 37i
12		0	0	E01-MV	8	E02-MV	9	4/0 AWG	2846	0.02726	0.01148	0.00000	0.00031	0.00000	0.00031	31.162105905401 9-13.121322679290 7i
13		0	0	E02-MV	9	D01-MV	10	500 kcmil	4679	0.01966	0.01690	0.00000	0.00066	0.00000	0.00066	29.245950569195 9-25.151517489508 4i
14		0	0	D01-MV	10	JB1-1	12	500 kcmil	1563	0.00657	0.00565	0.00000	0.00022	0.00000	0.00022	87.550737500491 -75.293634250422 3i
15		0	0	D02-MV	11	JB1-1	12	4/0 AWG	70	0.00067	0.00028	0.00000	0.00001	0.00000	0.00001	1266.96219152534 -533.47549064658 8i
16		0	0	JB1-1	12	D03-MV	13	750 kcmil	1549	0.00482	0.00534	0.00000	0.00025	0.00000	0.00025	93.217562682085 5-103.27399165515 8i
17		0	0	D03-MV	13	MVBUS1	116	1000 kcmil	1509	0.00342	0.00494	0.00000	0.00028	0.00000	0.00028	94.661431715928 7-136.69482481727 9i
18	Feeder #2	0.03465	0.01423	C01-LV	14	C01-MV	20	transformer	transformer	0.27001	2.70080	0.00079008	-0.00790	-0.00077081	0.00771	0.036650026586267 8-0.3665972236049 7i
19		0.03465	0.01423	B01-LV	15	B01-MV	21	transformer	transformer	0.29077	2.90846	0	0.00000	0	0.00000	0.034033193098201 4-0.3404219658843 9i
20		0.03465	0.01423	B02-LV	16	B02-MV	22	transformer	transformer	0.29077	2.90846	0	0.00000	0	0.00000	0.034033193098201 4-0.3404219658843 9i
21		0.03465	0.01423	B03-LV	17	B03-MV	23	transformer	transformer	0.29077	2.90846	0	0.00000	0	0.00000	0.034033193098201 4-0.3404219658843 9i
22		0.03465	0.01423	C02-LV	18	C02-MV	24	transformer	transformer	0.29077	2.90846	0	0.00000	0	0.00000	0.034033193098201 4-0.3404219658843 9i
23		0.03465	0.01423	C03-LV	19	C03-MV	25	transformer	transformer	0.29077	2.90846	0	0.00000	0	0.00000	0.034033193098201 4-0.3404219658843 9i
24		0	0	C01-MV	20	B01-MV	21	1/0 AWG	4078	0.08154	0.01850	0.00000	0.00036	0.00000	0.00036	11.663414423333 7-2.646405157075 38i
25		0	0	B01-MV	21	B02-MV	22	4/0 AWG	1854	0.01776	0.00748	0.00000	0.00020	0.00000	0.00020	47.835681449176 7-20.142088162142 i
26		0	0	B02-MV	22	B03-MV	23	500 kcmil	1850	0.00777	0.00668	0.00000	0.00026	0.00000	0.00026	73.968542007171 6-63.612946126167 6i
27		0	0	B03-MV	23	C02-MV	24	500 kcmil	3747	0.01574	0.01354	0.00000	0.00053	0.00000	0.00053	36.520363681149 5-31.407512765788 6i
28		0	0	C02-MV	24	C03-MV	25	750 kcmil	2205	0.00686	0.00760	0.00000	0.00036	0.00000	0.00036	65.484809339932 2-72.549393684281 i
29		0	0	C03-MV	25	MVBUS1	116	1000 kcmil	6431	0.01459	0.02107	0.00000	0.00120	0.00000	0.00120	22.211802279480 2-32.074714764309 5i
30	Feeder #3	0	0	C04-LV	26	C04-MV	31	transformer	transformer	0.29077	2.90846	0	0.00000	0	0.00000	0.034033193098201 4-0.3404219658843 9i
31		0.03465	0.01423	C05-LV	27	C05-MV	32	transformer	transformer	0.29077	2.90846	0	0.00000	0	0.00000	0.034033193098201 4-0.3404219658843 9i
32		0.03465	0.01423	C06-LV	28	C06-MV	33	transformer	transformer	0.27001	2.70080	0.00079008	-0.00790	-0.00077081	0.00771	0.036650026586267 8-0.3665972236049 7i
33		0.03465	0.01423	C07-LV	29	C07-MV	34	transformer	transformer	0.29077	2.90846	0	0.00000	0	0.00000	0.034033193098201 4-0.3404219658843 9i
34		0.03465	0.01423	C08-LV	30	C08-MV	35	transformer	transformer	0.29077	2.90846	0	0.00000	0	0.00000	0.034033193098201 4-0.3404219658843 9i
35		0	0	C04-MV	31	C05-MV	32	4/0 AWG	940	0.00900	0.00379	0.00000	0.00010	0.00000	0.00010	94.348248350784 -39.726898239639 6i
36		0	0	C05-MV	32	C06-MV	33	4/0 AWG	1460	0.01398	0.00589	0.00000	0.00016	0.00000	0.00016	60.744762607379 2-25.577592017302 2i
37		0	0	C06-MV	33	C07-MV	34	500 kcmil	937	0.00394	0.00339	0.00000	0.00013	0.00000	0.00013	146.04247882889 -125.59653183928 5i
38		0	0	C07-MV	34	C08-MV	35	500 kcmil	1343	0.00564	0.00485	0.00000	0.00019	0.00000	0.00019	101.892630464086 -87.627662199113 8i
39		0	0	C08-MV	35	MVBUS1	116	750 kcmil	3354	0.01043	0.01155	0.00000	0.00055	0.00000	0.00055	43.051283421154 -47.695710516946 9i
40	Feeder #4	0.03465	0.01423	B06-LV	36	B06-MV	43	transformer	transformer	0.27001	2.70080	0.00079008	-0.00790	-0.00077081	0.00771	0.036650026586267 8-0.3665972236049 7i
41		0.03465	0.01423	B07-LV	37	B07-MV	44	transformer	transformer	0.29077	2.90846	0	0.00000	0	0.00000	0.034033193098201 4-0.3404219658843 9i

Figure 3.5 Overview Inputs

Subsection 2 - Outputs

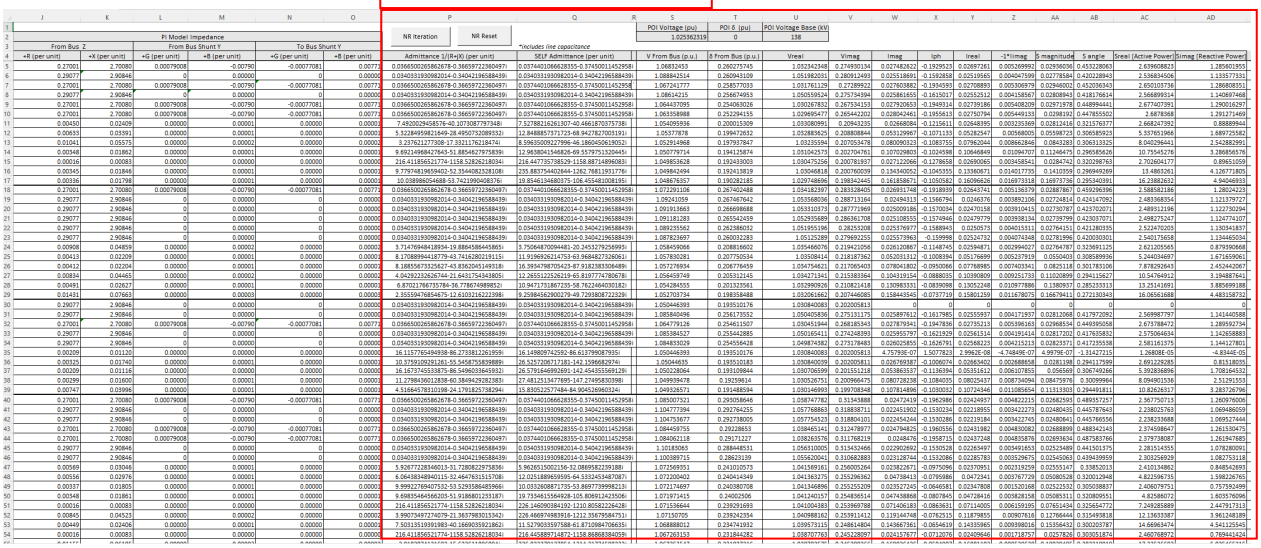

Figure 3.6 Overview Calculations

The second subsection of the "Overview" tab is the calculated values. For each "From Bus" to each "To Bus" the "Overview" tab calculates the admittance in column P. In Column Q, the tool pulls the self-admittance in per unit for each "From Bus" from the "Self-Admittance" sheet. Then in column S and T are the voltage magnitude and voltage phase angle for each "From Bus" for each iteration which are pulled from the "Δx" sheet. Columns U and V transfer this voltage phasor data from polar to rectangular. These voltages are then used in the remaining columns in W through AD to calculate the flow of current, apparent power, real power and reactive power between each of the "From Bus" and "To Bus". In the "POI Voltage (pu)", "POI δ (pu)" and "POI Voltage Base" cells the user inputs information on the target voltage for the wind farm's grid interconnection to the transmission system. For modeling, the "POI Voltage (pu)" is the voltage setpoint target for the site, the "POI δ (pu)" is set to zero since this is the slack bus, and the "POI Voltage Base" is set to 100MVA to match system base. Finally, the "NR Iteration" pushbutton will input the voltage values in rows S and T from the past iteration of Newton-Raphson solved voltage angles and magnitudes. The "NR Reset" pushbutton will revert all voltage magnitudes back to 1pu and all voltage phase angles to 0 degrees.

The next sheet of the excel tool is the "Self-Admittance" sheet in the tool which is used to calculate

the self-admittance of each wind farm bus.

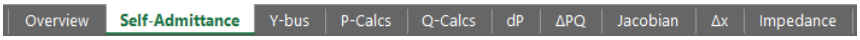

Figure 3.7 Self-Admittance Section

No user input is required on this sheet and the self-admittance of each "From Bus" is calculated provided back to Column Q of the Overview" sheet. The self-admittance is automatically calculated in this sheet by comparing each column bus number to the "From Bus" and "To Bus" columns on the Overview tab. If there is a match in either bus number column of the "Overview" sheet, then the equations sum the admittance of that row and add the shunt admittance for the respective bus. Then the "Total Self Admittance" row sums the admittances to arrive at the total self-admittance of that node. Nodes without a physical connection to one another will have a 0 in their respective cell.

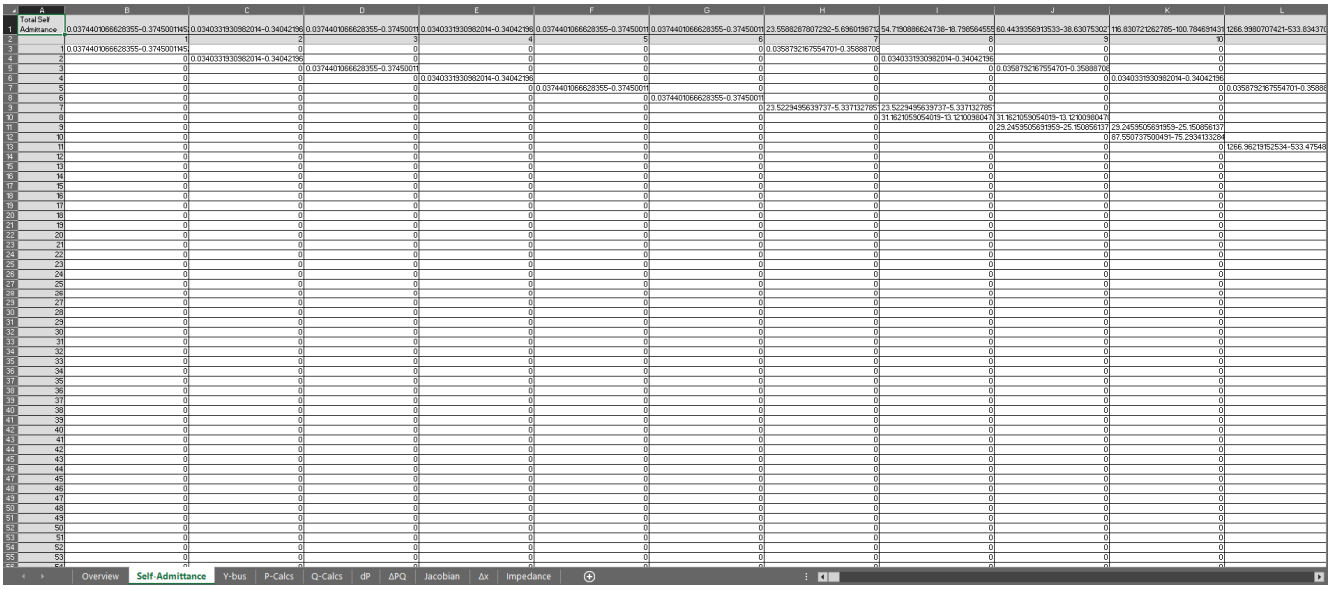

Figure 3.8 Self-Admittance Sheet

The next sheet of the excel tool is the Y-bus section which is used to calculate the admittance matrix for use in the Newton-Raphson equations.

Figure 3.9 Y-Bus Section

The admittance matrix is calculated by taking the negative admittance for off-diagonal elements and for the diagonal elements adding the admittances for any elements connected to that row/column number in addition to adding the susceptance for the row/column bus number.

$$Y = \begin{pmatrix} y_1 + y_{12} + y_{13} & -y_{12} & -y_{13} \\ -y_{12} & y_2 + y_{12} + y_{23} & -y_{23} \\ -y_{13} & -y_{23} & y_3 + y_{13} + y_{23} \end{pmatrix}$$

Figure 3.10 Y-Bus Formation

The Y-bus sheet is shown in the figure below where the admittance matrix is formulated based on the input data provided.

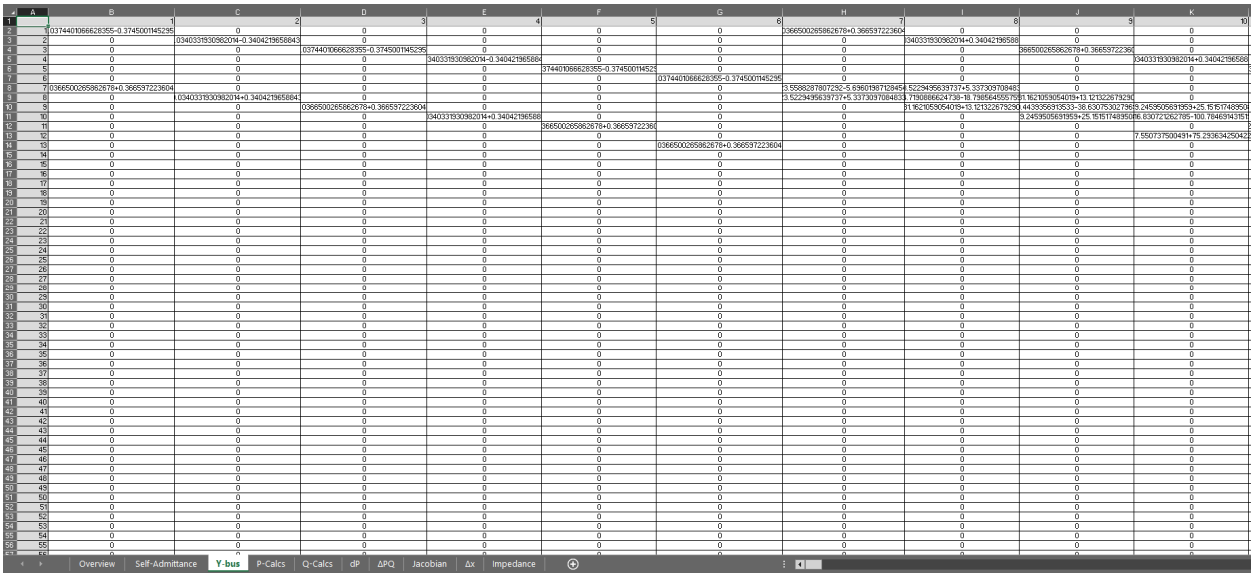

Figure 3.11 Y-Bus Sheet

The next sheet is the "P-Calcs" and "Q-Calcs" sheets. The "P-Calcs" calculates the real power at the respective bus number. The "Q-Calcs" calculates the reactive power at the respective bus number.

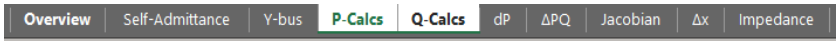

Figure 3.12 P-Calcs and Q-Calcs Section

Equations (2) and (3) provided earlier in this Thesis are used in the P-Calcs and Q-Calcs, respectively. These sheets also have the initial value assumptions built into the sheets for initial 1pu voltage magnitude and 0 deg. voltage phase angle.

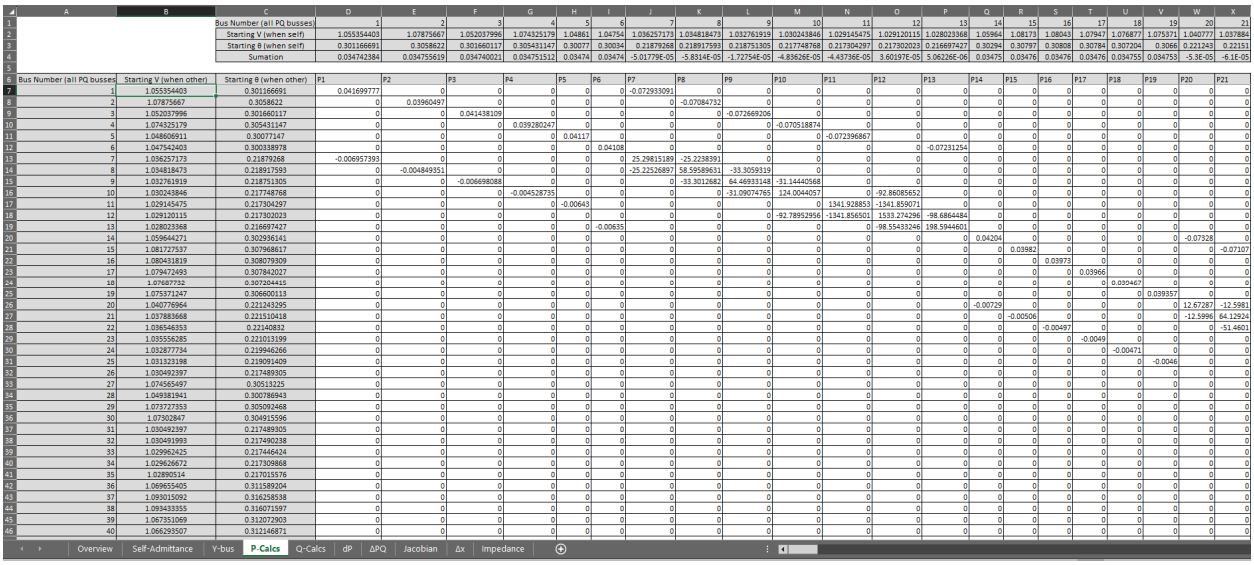

		Bus Number (all PQ busses)	1	2	3	4	5	6	7	8	9	10	11	12	13	14	15	16	17	18	19	20	21
		Starting V (when self)	1.055354403	1.07875667	1.052037996	1.074325179	1.04861	1.04754	1.036257173	1.034818473	1.032761919	1.030243846	1.029145475	1.029120115	1.028023368	1.05964	1.08173	1.08043	1.07947	1.076877	1.075371	1.040777	1.037884
		Starting θ (when self)	0.301166691	0.3058622	0.301660117	0.305431147	0.30077	0.30034	0.21879268	0.218917593	0.218751305	0.217748768	0.217304297	0.217302023	0.216697427	0.30294	0.30797	0.30808	0.30784	0.307204	0.3066	0.221243	0.22151
		Sumation	0.034742384	0.034755619	0.034740021	0.034751512	0.03474	0.03474	-5.01779E-05	-5.8314E-05	-1.72754E-05	-4.83626E-05	-4.43736E-05	3.60197E-05	5.06226E-06	0.03475	0.03476	0.03476	0.03476	0.034755	0.034753	-5.3E-05	-6.1E-05
	Bus Number (all PQ busses	Starting V (when other)	Starting θ (when other)	P1	P2	P3	P4	P5	P6	P7	P8	P9	P10	P11	P12	P13	P14	P15	P16	P17	P18	P19	P20	P21
7	1	1.055354403	0.301166691	0.041699777	0	0	0	0	0	-0.072933091	0	0	0	0	0	0	0	0	0	0	0	0	0	0
8	2	1.07875667	0.3058622	0	0.03960497	0	0	0	0	0	-0.07084732	0	0	0	0	0	0	0	0	0	0	0	0	0
9	3	1.052037996	0.301660117	0	0	0.041438109	0	0	0	0	0	-0.072669206	0	0	0	0	0	0	0	0	0	0	0	0
10	4	1.074325179	0.305431147	0	0	0	0.039280247	0	0	0	0	0	-0.070518874	0	0	0	0	0	0	0	0	0	0	0
11	5	1.048606911	0.30077147	0	0	0	0	0.04117	0	0	0	0	0	-0.072396867	0	0	0	0	0	0	0	0	0	0
12	6	1.047542403	0.300338978	0	0	0	0	0	0.04108	0	0	0	0	0	0	-0.07231254	0	0	0	0	0	0	0	0
13	7	1.036257173	0.21879268	-0.006957393	0	0	0	0	0	25.29815189	-25.2238391	0	0	0	0	0	0	0	0	0	0	0	0	0
14	8	1.034818473	0.218917593	0	-0.004849351	0	0	0	0	-25.22526897	58.59589631	-33.3059319	0	0	0	0	0	0	0	0	0	0	0	0
15	9	1.032761919	0.218751305	0	0	-0.006698088	0	0	0	0	-33.3012682	64.44933148	-31.14440568	0	0	0	0	0	0	0	0	0	0	0
16	10	1.030243846	0.217748768	0	0	0	-0.004528735	0	0	0	0	-31.09074765	124.0044057	0	-92.86085652	0	0	0	0	0	0	0	0	0
17	11	1.029145475	0.217304297	0	0	0	0	-0.00643	0	0	0	0	0	1341.928853	-1341.859071	0	0	0	0	0	0	0	0	0
18	12	1.029120115	0.217302023	0	0	0	0	0	0	0	0	0	-92.78952956	-1341.856501	1533.274296	-98.6864484	0	0	0	0	0	0	0	0
19	13	1.028023368	0.216697427	0	0	0	0	0	-0.00635	0	0	0	0	0	-98.55433246	198.5944601	0	0	0	0	0	0	0	0
20	14	1.05964271	0.30294143	0	0	0	0	0	0	0	0	0	0	0	0	0	0.04204	0	0	0	0	0	-0.07328	0
21	15	1.081727537	0.307968617	0	0	0	0	0	0	0	0	0	0	0	0	0	0	0.03982	0	0	0	0	0	-0.07107
22	16	1.080431819	0.308079309	0	0	0	0	0	0	0	0	0	0	0	0	0	0	0	0.03973	0	0	0	0	0
23	17	1.079472493	0.307842027	0	0	0	0	0	0	0	0	0	0	0	0	0	0	0	0	0.03966	0	0	0	0
24	18	1.07687732	0.307204415	0	0	0	0	0	0	0	0	0	0	0	0	0	0	0	0	0	0.039467	0	0	0
25	19	1.075371247	0.306600113	0	0	0	0	0	0	0	0	0	0	0	0	0	0	0	0	0	0	0.039357	0	0
26	20	1.040776964	0.221243295	0	0	0	0	0	0	0	0	0	0	0	0	-0.00729	0	0	0	0	0	0	12.67287	-12.5981
27	21	1.037883668	0.221510418	0	0	0	0	0	0	0	0	0	0	0	0	0	0	-0.00506	0	0	0	0	-12.5996	64.12924
28	22	1.036546353	0.22140832	0	0	0	0	0	0	0	0	0	0	0	0	0	0	0	-0.00497	0	0	0	0	-51.4601
29	23	1.035556285	0.221013199	0	0	0	0	0	0	0	0	0	0	0	0	0	0	0	0	-0.0049	0	0	0	0
30	24	1.032877734	0.219946266	0	0	0	0	0	0	0	0	0	0	0	0	0	0	0	0	0	-0.00471	0	0	0
31	25	1.031323198	0.219091409	0	0	0	0	0	0	0	0	0	0	0	0	0	0	0	0	0	0	-0.0046	0	0
32	26	1.030492397	0.217489305	0	0	0	0	0	0	0	0	0	0	0	0	0	0	0	0	0	0	0	0	0
33	27	1.074565497	0.30513225	0	0	0	0	0	0	0	0	0	0	0	0	0	0	0	0	0	0	0	0	0
34	28	1.049381941	0.300786943	0	0	0	0	0	0	0	0	0	0	0	0	0	0	0	0	0	0	0	0	0
35	29	1.073727353	0.305092468	0	0	0	0	0	0	0	0	0	0	0	0	0	0	0	0	0	0	0	0	0
36	30	1.07302847	0.304915596	0	0	0	0	0	0	0	0	0	0	0	0	0	0	0	0	0	0	0	0	0
37	31	1.030492397	0.217489305	0	0	0	0	0	0	0	0	0	0	0	0	0	0	0	0	0	0	0	0	0
38	32	1.030491993	0.217490238	0	0	0	0	0	0	0	0	0	0	0	0	0	0	0	0	0	0	0	0	0
39	33	1.029962425	0.217446424	0	0	0	0	0	0	0	0	0	0	0	0	0	0	0	0	0	0	0	0	0
40	34	1.029626672	0.217309868	0	0	0	0	0	0	0	0	0	0	0	0	0	0	0	0	0	0	0	0	0
41	35	1.02890514	0.217015576	0	0	0	0	0	0	0	0	0	0	0	0	0	0	0	0	0	0	0	0	0
42	36	1.069655405	0.311589204	0	0	0	0	0	0	0	0	0	0	0	0	0	0	0	0	0	0	0	0	0
43	37	1.093015092	0.316258538	0	0	0	0	0	0	0	0	0	0	0	0	0	0	0	0	0	0	0	0	0
44	38	1.093433355	0.316071597	0	0	0	0	0	0	0	0	0	0	0	0	0	0	0	0	0	0	0	0	0
45	39	1.067351069	0.312072903	0	0	0	0	0	0	0	0	0	0	0	0	0	0	0	0	0	0	0	0	0
46	40	1.066293507	0.312146871	0	0	0	0	0	0	0	0	0	0	0	0	0	0	0	0	0	0	0	0	0

Overview | Self-Admittance | Y-bus | P-Calcs | Q-Calcs | dP | ΔPQ | Jacobian | Δx | Impedance

Figure 3.13 P-Calcs Sheet

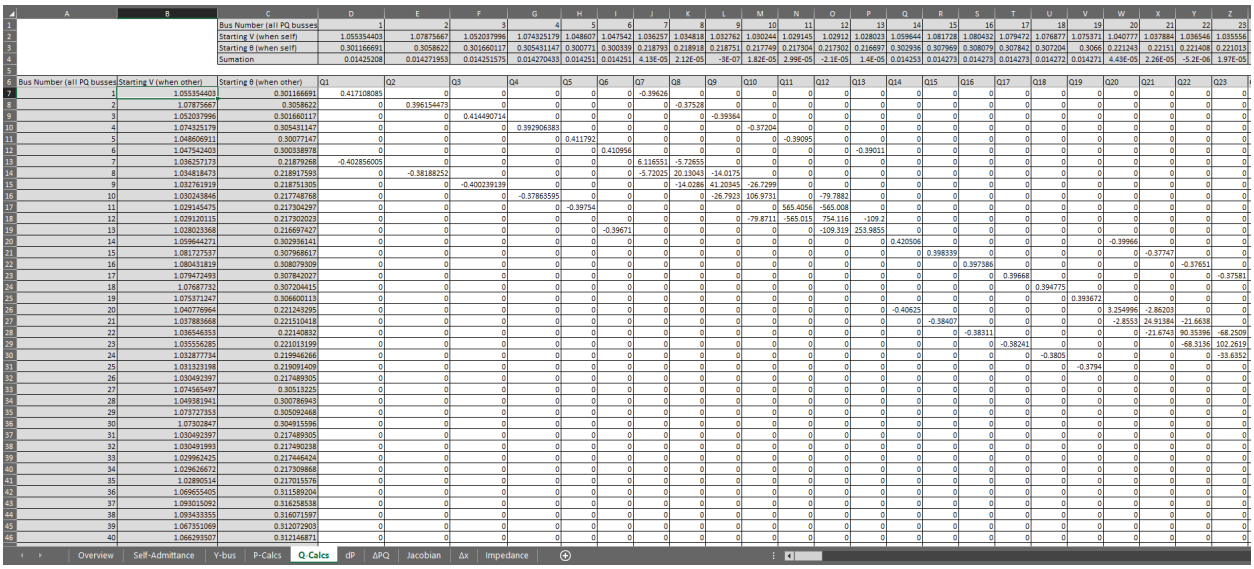

		Bus Number (all PQ busses	1	2	3	4	5	6	7	8	9	10	11	12	13	14	15	16	17	18	19	20	21	22	23
		Starting V (when self)	1.055354403	1.07875667	1.052037996	1.074325179	1.048607	1.047542	1.036257	1.034818	1.032762	1.030244	1.029145	1.02912	1.028023	1.059644	1.081728	1.080432	1.079472	1.076877	1.075371	1.040777	1.037884	1.036546	1.035556
		Starting θ (when self)	0.301166691	0.3058622	0.301660117	0.305431147	0.300771	0.300339	0.218793	0.218918	0.218751	0.217749	0.217304	0.217302	0.216697	0.302936	0.307969	0.308079	0.307842	0.307204	0.3066	0.221243	0.22151	0.221408	0.221013
		Sumation	0.01425208	0.014271953	0.014251575	0.014270433	0.014251	0.014251	4.13E-05	2.12E-05	-3E-07	1.82E-05	2.99E-05	-2.1E-05	1.4E-05	0.014253	0.014273	0.014273	0.014273	0.014272	0.014271	4.43E-05	2.26E-05	-5.2E-06	1.97E-05
	Bus Number (all PQ busses	Starting V (when other)	Starting θ (when other)	Q1	Q2	Q3	Q4	Q5	Q6	Q7	Q8	Q9	Q10	Q11	Q12	Q13	Q14	Q15	Q16	Q17	Q18	Q19	Q20	Q21	Q22	Q23
	1	1.055354403	0.301166691	0.417108085	0	0	0	0	0	-0.39626	0	0	0	0	0	0	0	0	0	0	0	0	0	0	0
	2	1.07875667	0.3058622	0	0.396154473	0	0	0	0	0	-0.37528	0	0	0	0	0	0	0	0	0	0	0	0	0	0
	3	1.052037996	0.301660117	0	0	0.414490714	0	0	0	0	0	-0.39364	0	0	0	0	0	0	0	0	0	0	0	0	0	0
	4	1.074325179	0.305431147	0	0	0	0.392906383	0	0	0	0	0	-0.37204	0	0	0	0	0	0	0	0	0	0	0	0	0
	5	1.048606911	0.30077147	0	0	0	0	0.411792	0	0	0	0	0	-0.39095	0	0	0	0	0	0	0	0	0	0	0	0
	6	1.047542403	0.300338978	0	0	0	0	0	0.410956	0	0	0	0	0	0	-0.39011	0	0	0	0	0	0	0	0	0	0
	7	1.096257179	0.21879268	-0.402856005	0	0	0	0	0	6.116551	-5.72655	0	0	0	0	0	0	0	0	0	0	0	0	0	0	0
	8	1.034818473	0.218917593	0	-0.38188252	0	0	0	0	-5.72025	20.13043	-14.0175	0	0	0	0	0	0	0	0	0	0	0	0	0	0
	9	1.032761919	0.218751305	0	0	-0.400239139	0	0	0	0	-14.0286	41.20345	-26.7299	0	0	0	0	0	0	0	0	0	0	0	0	0
	10	1.030243846	0.217748768	0	0	0	-0.37863595	0	0	0	0	-26.7923	106.9731	0	-79.7882	0	0	0	0	0	0	0	0	0	0	0
	11	1.029145475	0.217304297	0	0	0	0	-0.39754	0	0	0	0	0	565.4056	-565.008	0	0	0	0	0	0	0	0	0	0	0
	12	1.029120115	0.217302023	0	0	0	0	0	0	0	0	0	-79.8711	-565.015	754.116	-109.2	0	0	0	0	0	0	0	0	0	0
	13	1.028023368	0.216697427	0	0	0	0	0	-0.39671	0	0	0	0	0	-109.319	253.9855	0	0	0	0	0	0	0	0	0	0
	14	1.059644271	0.302936141	0	0	0	0	0	0	0	0	0	0	0	0	0	0.420506	0	0	0	0	0	0	-0.39966	0	0	0
	15	1.081727537	0.307968617	0	0	0	0	0	0	0	0	0	0	0	0	0	0	0.398339	0	0	0	0	0	-0.37747	0	0	0
	16	1.080431819	0.308079309	0	0	0	0	0	0	0	0	0	0	0	0	0	0	0	0.397386	0	0	0	0	0	-0.37651	0	0
	17	1.079472493	0.307842027	0	0	0	0	0	0	0	0	0	0	0	0	0	0	0	0	0.39668	0	0	0	0	0	-0.37581	0
	18	1.07687732	0.307204415	0	0	0	0	0	0	0	0	0	0	0	0	0	0	0	0	0	0.394775	0	0	0	0	0	0
	19	1.075371247	0.306600113	0	0	0	0	0	0	0	0	0	0	0	0	0	0	0	0	0	0	0.393672	0	0	0	0	0
	20	1.040776964	0.221243295	0	0	0	0	0	0	0	0	0	0	0	0	0	-0.40625	0	0	0	0	0	3.254996	-2.86203	0	0
	21	1.037883668	0.22151041	0	0	0	0	0	0	0	0	0	0	0	0	0	0	-0.38407	0	0	0	-2.8553	24.91384	-21.6638	0	0	0
	22	1.036546353	0.22140832	0	0	0	0	0	0	0	0	0	0	0	0	0	0	0	-0.38311	0	0	0	-21.6743	90.35396	-68.2509	0	0
	23	1.035556285	0.221013199	0	0	0	0	0	0	0	0	0	0	0	0	0	0	0	0	-0.38241	0	0	0	-68.3136	102.2619	0	0
	24	1.032877734	0.219946266	0	0	0	0	0	0	0	0	0	0	0	0	0	0	0	0	0	-0.3805	0	0	0	-33.6352	0	0
	25	1.031323198	0.219091409	0	0	0	0	0	0	0	0	0	0	0	0	0	0	0	0	0	0	-0.3794	0	0	0	0	0
	26	1.030492397	0.217489305	0	0	0	0	0	0	0	0	0	0	0	0	0	0	0	0	0	0	0	0	0	0	0	0
	27	1.074565497	0.30513225	0	0	0	0	0	0	0	0	0	0	0	0	0	0	0	0	0	0	0	0	0	0	0	0
	28	1.049381941	0.300786943	0	0	0	0	0	0	0	0	0	0	0	0	0	0	0	0	0	0	0	0	0	0	0	0
	29	1.073727353	0.305092468	0	0	0	0	0	0	0	0	0	0	0	0	0	0	0	0	0	0	0	0	0	0	0	0
	30	1.07302847	0.304915596	0	0	0	0	0	0	0	0	0	0	0	0	0	0	0	0	0	0	0	0	0	0	0	0
	31	1.030492397	0.217489305	0	0	0	0	0	0	0	0	0	0	0	0	0	0	0	0	0	0	0	0	0	0	0	0
	32	1.030491993	0.217490238	0	0	0	0	0	0	0	0	0	0	0	0	0	0	0	0	0	0	0	0	0	0	0	0
	33	1.029962425	0.217446424	0	0	0	0	0	0	0	0	0	0	0	0	0	0	0	0	0	0	0	0	0	0	0	0
	34	1.029626672	0.217309868	0	0	0	0	0	0	0	0	0	0	0	0	0	0	0	0	0	0	0	0	0	0	0	0
	35	1.02890514	0.217015576	0	0	0	0	0	0	0	0	0	0	0	0	0	0	0	0	0	0	0	0	0	0	0	0
	36	1.069655405	0.311589204	0	0	0	0	0	0	0	0	0	0	0	0	0	0	0	0	0	0	0	0	0	0	0	0
	37	1.093015092	0.316258538	0	0	0	0	0	0	0	0	0	0	0	0	0	0	0	0	0	0	0	0	0	0	0	0
	38	1.093433355	0.316071597	0	0	0	0	0	0	0	0	0	0	0	0	0	0	0	0	0	0	0	0	0	0	0	0
	39	1.067351069	0.312072903	0	0	0	0	0	0	0	0	0	0	0	0	0	0	0	0	0	0	0	0	0	0	0	0
	40	1.066293507	0.312146871	0	0	0	0	0	0	0	0	0	0	0	0	0	0	0	0	0	0	0	0	0	0	0	0

Overview | Self-Admittance | Y-bus | P-Calcs | Q-Calcs | dP | ΔPQ | Jacobian | Δx | Impedance

Figure 3.14 Q-Calcs Sheet

The next sheet is the "dP" sheet, which filters which buses within the wind farm are connected to one another.

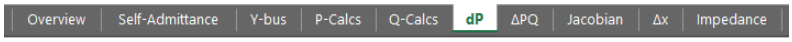

Figure 3.15 dP Section

The dP tab goes through the "P-Calcs" active power calculations and finds which buses connected to the header bus number are non-zero, which means there is some amount of power flow between the two and filters them as electrically connected. The only other function of this sheet is to them remove the bus number of the bus being evaluated. This filter is setup to work as long as no node has more than 10 connected buses and the Texas wind farm does not have more than this. Below is a snippet of this sheet.

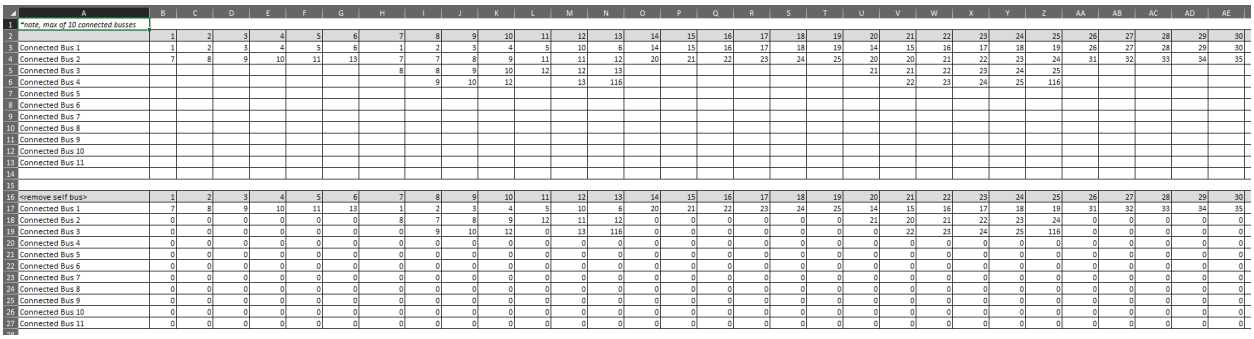

	A	B	C	D	E	F	G	H	I	J	K	L	M	N	O	P	Q	R	S	T	U	V	W	X	Y	Z	AA	AB	AC	AD	AE
1	*note, max of 10 connected busses																														
2		1	2	3	4	5	6	7	8	9	10	11	12	13	14	15	16	17	18	19	20	21	22	23	24	25	26	27	28	29	30
3	Connected Bus 1	1	2	3	4	5	6	1	2	3	4	5	10	6	14	15	16	17	18	19	14	15	16	17	18	19	26	27	28	29	30
4	Connected Bus 2	7	8	9	10	11	13	7	7	8	9	11	11	12	20	21	22	23	24	25	20	20	21	22	23	24	31	32	33	34	35
5	Connected Bus 3							8	8	9	10	12	12	13							21	21	22	23	24	25					
6	Connected Bus 4								9	10	12		13	116								22	23	24	25	116					
7	Connected Bus 5																														
8	Connected Bus 6																														
9	Connected Bus 7																														
10	Connected Bus 8																														
11	Connected Bus 9																														
12	Connected Bus 10																														
13	Connected Bus 11																														
14																															
15																															
16	<remove self bus>	1	2	3	4	5	6	7	8	9	10	11	12	13	14	15	16	17	18	19	20	21	22	23	24	25	26	27	28	29	30
17	Connected Bus 1	7	8	9	10	11	13	1	2	3	4	5	10	6	20	21	22	23	24	25	14	15	16	17	18	19	31	32	33	34	35
18	Connected Bus 2	0	0	0	0	0	0	8	7	8	9	12	11	12	0	0	0	0	0	0	21	20	21	22	23	24	0	0	0	0	0
19	Connected Bus 3	0	0	0	0	0	0	0	9	10	12	0	13	116	0	0	0	0	0	0	0	22	23	24	25	116	0	0	0	0	0
20	Connected Bus 4	0	0	0	0	0	0	0	0	0	0	0	0	0	0	0	0	0	0	0	0	0	0	0	0	0	0	0	0	0	0
21	Connected Bus 5	0	0	0	0	0	0	0	0	0	0	0	0	0	0	0	0	0	0	0	0	0	0	0	0	0	0	0	0	0	0
22	Connected Bus 6	0	0	0	0	0	0	0	0	0	0	0	0	0	0	0	0	0	0	0	0	0	0	0	0	0	0	0	0	0	0
23	Connected Bus 7	0	0	0	0	0	0	0	0	0	0	0	0	0	0	0	0	0	0	0	0	0	0	0	0	0	0	0	0	0	0
24	Connected Bus 8	0	0	0	0	0	0	0	0	0	0	0	0	0	0	0	0	0	0	0	0	0	0	0	0	0	0	0	0	0	0
25	Connected Bus 9	0	0	0	0	0	0	0	0	0	0	0	0	0	0	0	0	0	0	0	0	0	0	0	0	0	0	0	0	0	0
26	Connected Bus 10	0	0	0	0	0	0	0	0	0	0	0	0	0	0	0	0	0	0	0	0	0	0	0	0	0	0	0	0	0	0
27	Connected Bus 11	0	0	0	0	0	0	0	0	0	0	0	0	0	0	0	0	0	0	0	0	0	0	0	0	0	0	0	0	0	0

Figure 3.16 dP Sheet

The next sheet is "ΔPQ" which performs the calculations as listed in equation (10) to determine the change in active and reactive power between iterations.

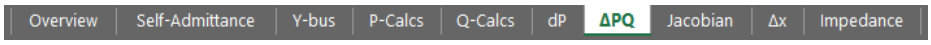

Figure 3.17 ΔPQ Section

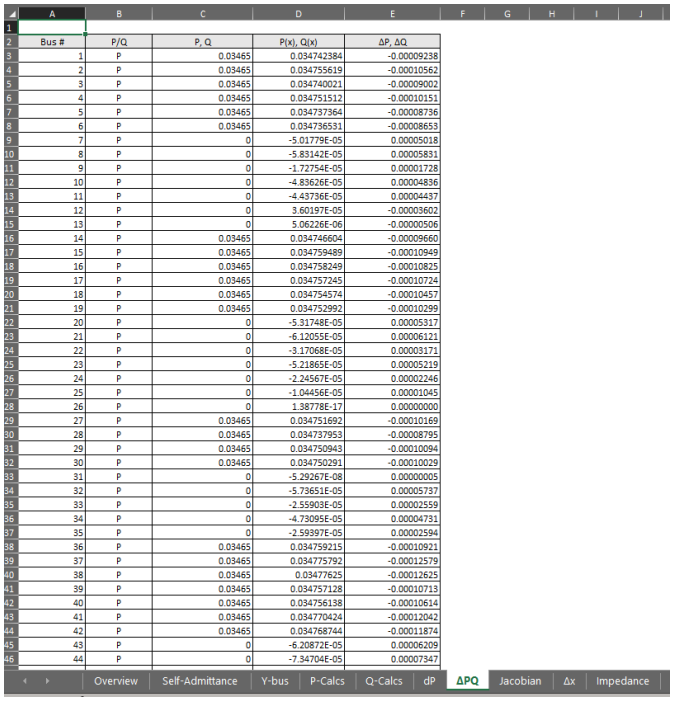

	A	B	C	D	E
1					
2	Bus #	P/Q	P, Q	P(x), Q(x)	ΔP, ΔQ
3	1	P	0.03465	0.034742384	-0.00009238
4	2	P	0.03465	0.034755619	-0.00010562
5	3	P	0.03465	0.034740021	-0.00009002
6	4	P	0.03465	0.034751512	-0.00010151
7	5	P	0.03465	0.034737364	-0.00008736
8	6	P	0.03465	0.034736531	-0.00008653
9	7	P	0	-5.01779E-05	0.00005018
10	8	P	0	-5.83142E-05	0.00005831
11	9	P	0	-1.72754E-05	0.00001728
12	10	P	0	-4.83626E-05	0.00004836
13	11	P	0	-4.43736E-05	0.00004437
14	12	P	0	3.60197E-05	-0.00003602
15	13	P	0	5.06226E-06	-0.00000506
16	14	P	0.03465	0.034746604	-0.00009660
17	15	P	0.03465	0.034759489	-0.00010949
18	16	P	0.03465	0.034758249	-0.00010825
19	17	P	0.03465	0.034757245	-0.00010724
20	18	P	0.03465	0.034754574	-0.00010457
21	19	P	0.03465	0.034752992	-0.00010299
22	20	P	0	-5.31748E-05	0.00005317
23	21	P	0	-6.12055E-05	0.00006121
24	22	P	0	-3.17068E-05	0.00003171
25	23	P	0	-5.21865E-05	0.00005219
26	24	P	0	-2.24567E-05	0.00002246
27	25	P	0	-1.04456E-05	0.00001045
28	26	P	0	1.38778E-17	0.00000000
29	27	P	0.03465	0.034751692	-0.00010169
30	28	P	0.03465	0.034737953	-0.00008795
31	29	P	0.03465	0.034750943	-0.00010094
32	30	P	0.03465	0.034750291	-0.00010029
33	31	P	0	-5.29267E-08	0.00000005
34	32	P	0	-5.73651E-05	0.00005737
35	33	P	0	-2.55903E-05	0.00002559
36	34	P	0	-4.73095E-05	0.00004731
37	35	P	0	-2.59397E-05	0.00002594
38	36	P	0.03465	0.034759215	-0.00010921
39	37	P	0.03465	0.034775792	-0.00012579
40	38	P	0.03465	0.03477625	-0.00012625
41	39	P	0.03465	0.034757128	-0.00010713
42	40	P	0.03465	0.034756138	-0.00010614
43	41	P	0.03465	0.034770424	-0.00012042
44	42	P	0.03465	0.034768744	-0.00011874
45	43	P	0	-6.20872E-05	0.00006209
46	44	P	0	-7.34704E-05	0.00007347

Overview | Self-Admittance | Y-bus | P-Calcs | Q-Calcs | dP | ΔPQ | Jacobian | Δx | Impedance

Figure 3.18 ΔPQ Sheet

The next sheet is the most complex part of the Excel tool which is the "Jacobian" sheet. It calculates the Jacobian matrix for the system consisting of partial derivatives.

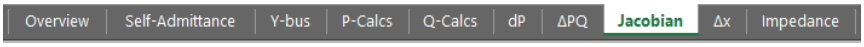

Figure 3.19 Jacobian Section

This sheet follows equation (11) previously provided. As opposed to more complex processing of partial derivatives, this Excel tool linearizes the equations in (11) to the equations listed below in Figure 3.20.

$$\frac{\partial P_i}{\partial \delta_k} = V_i V_k G_{ik} \sin(\delta_i - \delta_k) - V_i V_k B_{ik} \cos(\delta_i - \delta_k)$$

$$\frac{\partial P_i}{\partial V_k} = V_i G_{ik} \cos(\delta_i - \delta_k) + V_i B_{ik} \sin(\delta_i - \delta_k)$$

$$\frac{\partial Q_i}{\partial \delta_k} = -V_i V_k B_{ik} \sin(\delta_i - \delta_k) - V_i V_k G_{ik} \cos(\delta_i - \delta_k)$$

$$\frac{\partial P_i}{\partial \delta_i} = \sum_{j=1}^{n} -V_i V_j G_{ij} \sin(\delta_i - \delta_k) + V_i V_j B_{ij} \cos(\delta_i - \delta_k)$$

$$\frac{\partial P_i}{\partial V_i} = 2V_i G_{ii} + \sum_{j=1}^{n} V_k G_{ik} \cos(\delta_i - \delta_k) + V_k B_{ik} \cos(\delta_i - \delta_k)$$

$$\frac{\partial Q_i}{\partial \delta_i} = \sum_{j=1}^{n} V_i V_j B_{ij} \sin(\delta_i - \delta_k) + V_i V_j G_{ij} \cos(\delta_i - \delta_k)$$

Figure 3.20 Jacobian Matrix Equations

The excel tool then uses the below matrix setup in Excel with color coding shown in Figure 3.21 below to identify in the tool which formula and respective partial derivative is being evaluated. Each cell looks at the 10 possible connected buses in "dP" to automatically execute the Jacobian matrix equations.

δP1/δθ1	δP1/δθ2	…δP1/δθN	δP1/δV1	δP1/δV2	…..δP1/δVN
δP2/δθ1	δP2/δθ2	…δP2/δθN	δP2/δV1	δP2/δV2	…δP2/δVN
…..δPN/δθ1	….δPN/δθ2	…δPN/δθN	…δPN/δV2	…δPN/δV2	…..δP2/δVN
δQ1/δθ1	δQ1/δθ2	…δQ1/δθN	δQ1/δV1	δQ1/δV2	…..δQ1/δVN
δQ2/δθ1	δQ2/δθ2	…δQ2/δθN	δQ2/δV1	δQ2/δV2	…δQ2/δVN
…δQN/δθ1	…δQN/δθ2	…δQN/δθN	…δQN/δV2	…δQN/δV2	…..δQ2/δVN

Figure 3.21 Jacobian Matrix

The next sheet in the excel tool is the Δx sheet which where the final n+1 iteration for the voltage magnitude and phase angle are calculated.

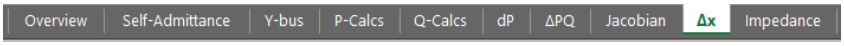

Figure 3.22 Δx Section

This sheet uses equation (13) to invert the Jacobian Matrix and multiply the result by the ΔPQ matrix to arrive at the new voltage magnitude and phase angle quantities. The previous iteration, or initialized values, are pulled into the C column. The previous voltage angle or magnitude is then added to the new change in voltage angle or magnitude, respectively. This follows equation (14) and provides the updated voltage angle and magnitude after an iteration of Newton-Raphson. The Sheet requires no user input and is shown in the figure below.

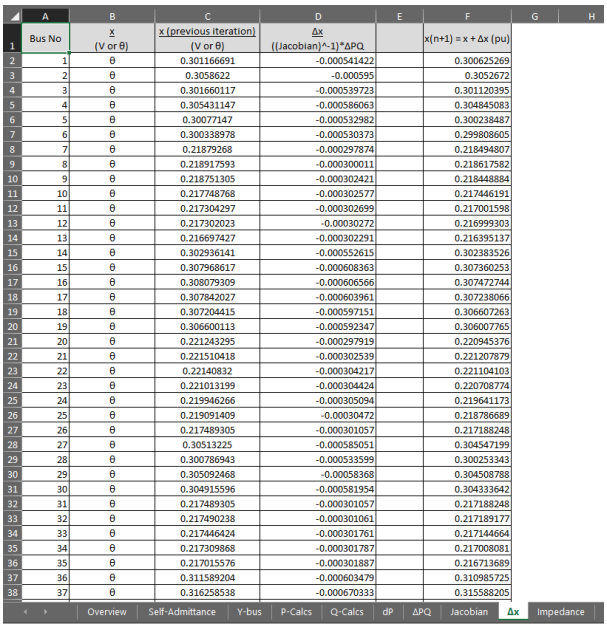

	A	B	C	D	E	F	G	H
1	Bus No	x (V or θ)	x (previous iteration) (V or θ)	Δx ((Jacobian)^-1)*ΔPQ		x(n+1) = x + Δx (pu)		
2	1	θ	0.301166691	-0.000541422		0.300625269		
3	2	θ	0.3058622	-0.000595		0.3052672		
4	3	θ	0.301660117	-0.000539723		0.301120395		
5	4	θ	0.305431147	-0.000586063		0.304845083		
6	5	θ	0.30077147	-0.000532982		0.300238487		
7	6	θ	0.30033897 8	-0.000530373		0.299808605		
8	7	θ	0.21879268	-0.000297874		0.218494807		
9	8	θ	0.218917593	-0.000300011		0.218617582		
10	9	θ	0.218751305	-0.000302421		0.218448884		
11	10	θ	0.217748768	-0.000302577		0.217446191		
12	11	θ	0.217304297	-0.000302699		0.217001598		
13	12	θ	0.217302023	-0.00030272		0.216999303		
14	13	θ	0.216697427	-0.000302291		0.216395137		
15	14	θ	0.302936141	-0.000552615		0.302383526		
16	15	θ	0.307968617	-0.000608363		0.307360253		
17	16	θ	0.308079309	-0.000606566		0.307472744		
18	17	θ	0.307842027	-0.000603961		0.307238066		
19	18	θ	0.307204415	-0.000597151		0.306607263		
20	19	θ	0.306600113	-0.000592347		0.306007765		
21	20	θ	0.221243295	-0.000297919		0.220945376		
22	21	θ	0.221510418	-0.000302539		0.221207879		
23	22	θ	0.22140832	-0.000304217		0.221104103		
24	23	θ	0.221013199	-0.000304424		0.220708774		
25	24	θ	0.219946266	-0.000305094		0.219641173		
26	25	θ	0.219091409	-0.00030472		0.218786689		
27	26	θ	0.217489305	-0.000301057		0.217188248		
28	27	θ	0.30513225	-0.000585051		0.304547199		
29	28	θ	0.300786943	-0.000533599		0.300253343		
30	29	θ	0.305092468	-0.00058368		0.304508788		
31	30	θ	0.304915596	-0.000581954		0.304333642		
32	31	θ	0.217489305	-0.000301057		0.217188248		
33	32	θ	0.217490238	-0.000301061		0.217189177		
34	33	θ	0.217446424	-0.000301761		0.217144664		
35	34	θ	0.217309868	-0.000301787		0.217008081		
36	35	θ	0.217015576	-0.000301887		0.216713689		
37	36	θ	0.311589204	-0.000603479		0.310985725		
38	37	θ	0.316258538	-0.000670333		0.315588205		

Overview | Self-Admittance | Y-bus | P-Calcs | Q-Calcs | dP | ΔPQ | Jacobian | Δx | Impedance

Figure 3.23 Δx Sheet

The updated values angles and magnitudes are automatically populated back into the "Overview" sheet Columns P and Q which are respectively the "V From Bus (p.u.)" and "δ From Bus (p.u.)". The current and power values in the "Overview" sheet now represent the n+1 iteration. The final sheet in the Excel tool is the "Impedance" sheet.

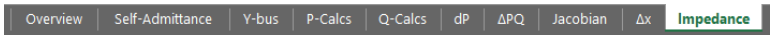

Figure 3.24 Impedance Section

This section holds the cable and transformer impedance data which is provided as an input to the tool. Additionally, this sheet holds the base values for per unit calculations, bus voltage magnitudes and phase angles for initializing the Newton-Raphson equations, and a holding area for the previous iteration quantities. New equipment can be added here as necessary to match actual wind farm equipment or specifics. Figure 3.25 below shows the main equipment used for the Texas wind farm model.

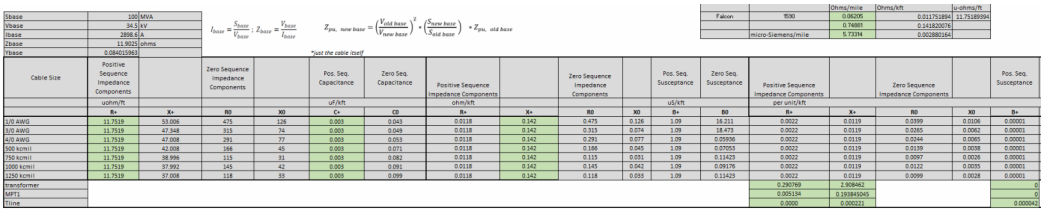

Sbase	100 MVA
Vbase	34.5 kV
Ibase	2898.6 A
Zbase	11.9025 ohms
Ybase	0.084015963

$$I_{base} = \frac{S_{base}}{V_{base}} ; Z_{base} = \frac{V_{base}}{I_{base}} \qquad Z_{pu,\ new\ base} = \left(\frac{V_{old\ base}}{V_{new\ base}}\right)^2 * \left(\frac{S_{new\ base}}{S_{old\ base}}\right) * Z_{pu,\ old\ base}$$

*just the cable itself

		Ohms/mile	Ohms/kft	u-ohms/ft
Falcon	1590	0.06205	0.011751894	11.75189394
		0.74581	0.141820076	
	micro-Siemens/mile	5.73374	0.002880164	

Cable Size	Positive Sequence Impedance Components		Zero Sequence Impedance Components		Pos. Seq. Capacitance	Zero Seq. Capacitance	Positive Sequence Impedance Components		Zero Sequence Impedance Components		Pos. Seq. Susceptance	Zero Seq. Susceptance	Positive Sequence Impedance Components		Zero Sequence Impedance Components		Pos. Seq. Susceptance
	uohm/ft				uF/kft		ohm/kft				uS/kft		per unit/kft				
	R+	X+	R0	X0	C+	C0	R+	X+	R0	X0	B+	B0	R+	X+	R0	X0	B+
1/0 AWG	11.7519	53.006	475	126	0.003	0.043	0.0118	0.142	0.475	0.126	1.09	16.211	0.0022	0.0119	0.0399	0.0106	0.00001
3/0 AWG	11.7519	47.348	315	74	0.003	0.049	0.0118	0.142	0.315	0.074	1.09	18.473	0.0022	0.0119	0.0265	0.0062	0.00001
4/0 AWG	11.7519	47.008	291	77	0.003	0.053	0.0118	0.142	0.291	0.077	1.09	0.05936	0.0022	0.0119	0.0244	0.0065	0.00001
500 kcmil	11.7519	42.008	166	45	0.003	0.071	0.0118	0.142	0.166	0.045	1.09	0.07053	0.0022	0.0119	0.0139	0.0038	0.00001
750 kcmil	11.7519	38.996	115	31	0.003	0.082	0.0118	0.142	0.115	0.031	1.09	0.11423	0.0022	0.0119	0.0097	0.0026	0.00001
1000 kcmil	11.7519	37.992	145	42	0.003	0.091	0.0118	0.142	0.145	0.042	1.09	0.09176	0.0022	0.0119	0.0122	0.0035	0.00001
1250 kcmil	11.7519	37.008	118	33	0.003	0.099	0.0118	0.142	0.118	0.033	1.09	0.11429	0.0022	0.0119	0.0099	0.0028	0.00001
transformer													0.290769	2.908462			0
MPT1													0.005134	0.193845045			0
Tline													0.0000	0.000221			0.000042

Figure 3.25 Impedance Sheet

This concludes the review of the model build of the excel tool. It is built to calculate power flow across the entire wind farm as well as provide the electrical losses incurred in the system for different operating points to provide insight into the plant design and operation.

3.3 Model Data Comparison to Real World Data

This section will review the model data output compared to the operational data at the wind farm for comparison. Real time telemetry was pulled from the wind farm historian for this comparison to be completed. This data was pulled from both the substation historian which receives DNP3 points from the substation and Modbus points from the WTGs. Hourly average data was collected for a period of one year ranging from 09/19/21 at midnight until 09/18/22 at 11PM. All time is given in central standard time zone and the time period goes from the time listed until the following hour.

There were hours of data omitted from the dataset for various reasons, mostly due to turbine maintenance or trips that occurred during the year of data under consideration. There were also time periods where a substation feeder circuit was out of service and those time periods were removed from the dataset. If a WTG was offline for more than 48 hours, the historical voltage at that WTG was set equal to the adjacent WTG, since there was no record of telemetry at the offline WTG. WTG C04 was offline the entire time of data collection. Figure 3.26 provides the time for each month of data along with a description of the time and reason the dataset was removed.

	Month 1 9/13/21 - 10/18/21	Month 2 10/19/21 - 11/18/21	Month 3 11/19/21 - 12/18/21	Month 4 12/19/21 - 1/18/22	Month 5 1/19/22 - 2/18/22	Month 6 2/19/22 - 3/18/22
High-level data description	OK	C10 offline second half of month. Matched C10 voltage to C09	C10 offline C10 voltage set equal to C09 (entire time period)	C10 offline C10 voltage set equal to C09 (first two days)	C09 offline. C09 voltage set equal to C10 (last 24hrs)	C09 offline. C09 voltage set equal to C10 (entire time period)
Total number of hourly data periods omitted	**23**	**141**	**51**	**157**	**117**	**34**
Event Numbers						
1	4 hrs - B02 outage 9/23/21 10AM-2PM	9 hrs - site outage 10/20 9am-6pm	6 hrs - E10 offline 11/24: 4-10PM	18 hrs - D12 turbine outage 12/19 2AM to 12/19 8PM	1hr - C16, C17, D10 outage,	2hrs - Feeder 4 offlin, 2/19/22 4-6PM
2	6 hrs - entire sub outage 10/8/212-8PM	1hr - B06 outage 10/29 12PM	2 hrs - D12 offline 11/25: 7-9PM	1hr - C06 outage 12/20 5PM	58 hrs - F10 outage, 1/25/22 9AM to 1/27/22 7PM	10hrs- All feeders offline 2/28 10AM-8PM
3	1 hr - C16 outage 10/11/21 11AM-noon	7 hrs - F11 outage 10/29 5PM to 11\1 3PM	2 hrs - F02 offline 11/28: 2-4PM	16 hrs - B10 outage 12/21 6PM - 10AM	4 hrs - C05 outage, 2/4/22 7-8AM, 9AM-noon	6hrs - Feeder 4 offline, 3/1 9AM-3PM
4	1 hr - C01 outage 10/11\21 1-2PM	53 hrs - F11 outage 11/3 10AM to 11/5 2PM	1 hr - Many turbines (all feeder 4) offline 11\30: 8-9AM	1 hr - F12 outage 12/23 11AM	7 hrs - C12, C14, C15, C16, C17, D09, D10 (feeder 4)outage, 2/10\22 9AM-4PM	2 hrs - B03 outage, 3/2\22 11AM-1PM
5	1 hr - D12 outage 10/11\21 4-5PM	3 hrs - F04 & E06 outage 11/8 10AM to 1PM	13 hrs - Many turbines (all feeder 4) offline 12/2 2PM - 12/3 9AM	1hr - F06 outage 12/28 9AM	9hrs - Feeder 7 and 1 outage, 2/11\22 9AM-6PM	4 hr - Feeder 4 outage, 3/3\22 noon-4PM
6	1 hr - C15 outage 10\15\21 noon-1PM	2 hrs - E10 outage 11\17 10AM-noon	19 hrs - Turbines D12 & B10 offline 12\6 2PM - 12\7 9AM	2 hrs - F09 outage 12\30 9-11AM	4 hrs - feeder 4 outage, 2\12\22 8AM - noon	1 hr - E02 outage, 3/8\22 2-3PM
7	2 hrs - E01 outage 10\16\21 9-11PM	2 hrs - D12 outage 11\18 6-8PM	1hr - B01 offline 12\10 10AM	2hs - F08 outage 1\4 12-2PM	7 hrs - feeder 2 and 3 outage, 2\13\22 9AM-4PM	1hr - sub offline, 3\12\22 9-10PM
8	6 hrs - E01 outage 10\17\21 5AM-11AM		1hr - C01 offline 12\10 1PM	2hrs - F11 outage 1\6 9-11AM	6 hrs - feeder 6 outage, 2\14\22 9AM - 3PM	1hr - E03 outage 3/13\22 2-3AM
9	1 hr - E01 outage 10\16\21 10-11AM			69 hrs - B6, B7, B9, B10 outage 1\8 11PM to 1\11 8PM	1hr - D03 outage, 2\16\22, noon-1PM	7hrs - B10 outage, 3/4\22 9AM-4PM
10				10 hrs - D12 outage 1\15 10PM to 1\16 8AM	19hrs - feeder 4 outage, 2\16\22 8PM - 3PM 2\17\22	
11				2 hrs - F07 outage 1\17 11-1PM	1hr -feeder 4 outage 2\19\22 4-5PM	
12				2 hrs - D12 outage 1\18 12-2PM		
13				3- hrs, B10 outage 12/22 10AM-11AM, NOON-2PM		
14				1hr - B10 outage 12/27 9-10AM		
15				15 hrs - B10 outage 12/28 10PM - 12/29 noon		
16				8 hrs - B10 outage 1\5\22 11AM-7PM		
17				3 hrs - B10 outage 1\7\22 10-1PM		
18				1hrs - B10 outage 1\11 8-9PM		

	Month 7 3/19/22 - 4/18/22	Month 8 4/19/22 - 5/18/22	Month 9 5/19/22 - 6/18/22	Month 10 6/19/22 - 7/18/22	Month 11 7/19/22 - 8/18/22	Month 12 8/19/22 - 9/18/22
High-level data description	C09 offline. C09 voltage set equal to C10 (entire time period)	OK	C05 offline second half of time period. C05 voltage set equal to C07 voltage (C06 has a tap change)	C05 offline for the first "week. C05 voltage set equal to C07 voltage (C06 has a tap change)	C12 outage "last week of data. Zero'd out these time periods at the end, feeder mostly out anyway	C12 outage entire time period -removed" first week of data as feeder was out. Then matched C12 voltage to C14 voltage for remainder of period
Total number of hourly data periods omitted	**123**	**78**	**185**	**13**	**144**	**227**
Event Numbers						
1	2 hrs - F02 outage, 3/23/22 2-4PM	1hr - C06 outage, 4/19\22 noon-1PM	1hr - D05 outage 5/15\22 10-11AM	1 hr - C01 outage 6/20\22 9-10AM	2 hrs - D11 outage 7/19\22 10AM-noon	89 hrs - C12 outage (feeder outage) 8/19\22 12AM - 8\22\22 5PM
2	8hrs - B10 outage 3/23\22 3AM-11AM	8 hrs - B10 outage, 4/21\22 9-5PM	11 hrs - B03 outage 5/25\22 1AM-noon	2 hrs - C08 outage 7\6\22 11-1PM	1 hr - D11 outage 7\20\22 9AM-10AM	1 hr - C01 outage 8/23\22 10-11AM
3	1hr - Feeder 4 outage, 3/25\22 3-4PM	1 hr - B10 line, 4\22\22 9-10AM	2 hrs - B06 outage 5\23\22 2-4PM	10 hrs - C10 outage 7\8\22 9PM - 7\9\22 7AM	1 hr - B01 outage 7\21\22 11-noon	2 hrs - C05 outage 8\27\22 4-6PM
4	6hrs - E03 outage, 3/31\22 9-3PM	7 hrs - B10 outage, 4\22\22, 11AM-6PM	154 hrs - substation outage (C05 issue) 5/30\22 7AM - 6\5\22 5PM		1 hr - B01 outage 7\21\22 2-3PM	13 hrs - C05 outage 8\29\22 8PM - 8\29\22 9AM
5	95hrs - F11 outage 4\1\22 11AM - 4\5\22 10AM	1hr - E06 offline, 4\28\22 10-11AM	4 hrs - C15 outage 6\6\22 1-5PM		1 hr - F03 outage 7\22\22 9-10AM	95 hrs - B07 outage 8\29\22 10AM - 9\2\22 9AM
6	2 hrs - E03 outage, 4\5\22 12-2PM	2 hr - D09 4\29\22 9-11AM	8 hrs - B01 outage 6\7\22 9-5PM		1 hr - C14 outage 7\28\22 9-10AM	7 hrs - Feeder 3 outage 9\8\22 9-4PM
7	2 hrs - D05 outage, 4\6\22 10-noon	3hrs - B03 outage 5\5\22 9-noon	1 hr - C10 outage 6\13\22 1-2PM		2 hrs - D04 outage 8\2\22 10-noon	20 hrs - C15 outage 9\9\22 noon - 9\10\22 7AM
8	2 hrs - D04 outage, 4\8\22 1-3PM	4 hrs - F04 outage 5\9\22 11-3PM	1 hr -F11 outage 6\6\22 noon-1PM		1 hr - C10 outage 8\9\22 10-11AM	
9	1 hr - C17 outage, 4\7\22 10-11AM	14 hrs - E01 outage 5\9\22 7PM - 5\10\22 9AM	2 hrs - F08 outage 5/26/22 10-noon;		1 hr - C05 outage 8\10\22 9-10AM	
10	2 hrs - B10 outage, 4\7\22 noon-2PM	24hrs - Feeder 3 outage 5\11\22 9AM - 5\12\22 9AM	1hr - F08 outage 5/26\22 1-2PM		133 hrs - feeder 5 outage 8\13\22 11AM - 8\18\22 midnight	
11	1 hr - B06 outage, 4\13\22 9-10AM	6 hrs - F09 outage 5\17\22 8-2PM				
12	1 hr - C05, C07, 4\18\22 10-11AM	6 hrs - B10 outage 4/23\22 8-2PM				
13		1 hr - B10 outage 4/27\22 10-11AM				

Figure 3.26 Texas Wind Farm Historical Data Set Omissions

After collecting the data from site and filtering for valid datasets, data was averaged for each month for comparison to data from the model. From each WTG the kW, kVAr, and voltage magnitude were all collected and averaged (voltage phase angle not available). For substation data the capacitor bank MVAr, MV bus voltage, MWs and MVAr for each 34.5kV feeder, transformer low-side MWs and MVAr, and transformer high-side MWs and MVAr were all collected and averaged.

After averaging out the operational data, each month's average real and reactive power values per WTG were input into the spreadsheet tool. Next the average POI voltage was input into the spreadsheet tool. Cap bank contribution was also set in the model to equal the average MVAr flow in per unit through the cap bank relay. Then the OLTC position was selected while performing Newton-Raphson iterations to regulate the MV bus voltage as close as possible to the monthly average MV bus voltage recorded.

The SCADA data from the Texas wind farm was used as inputs to the excel tool and the outputs of the model were compared to the SCADA data recorded in the field. The resulting MW and MVAr at the 138kV bus in the model verse the field data is provided in the figures below. As can

be seen the excel tool modeled the data with similar results to the field measured quantities.

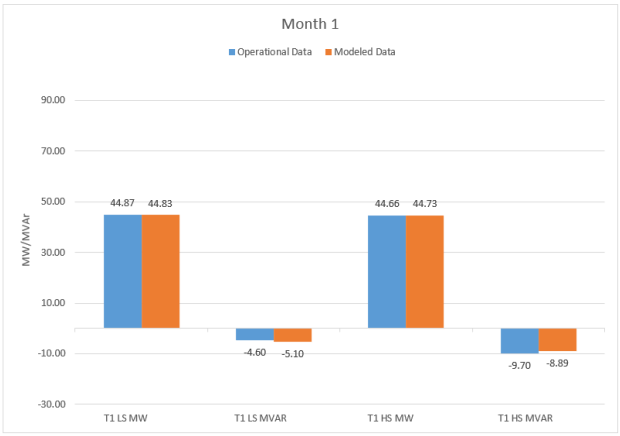

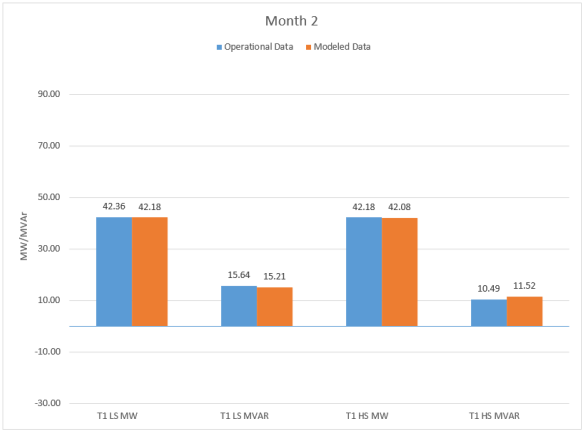

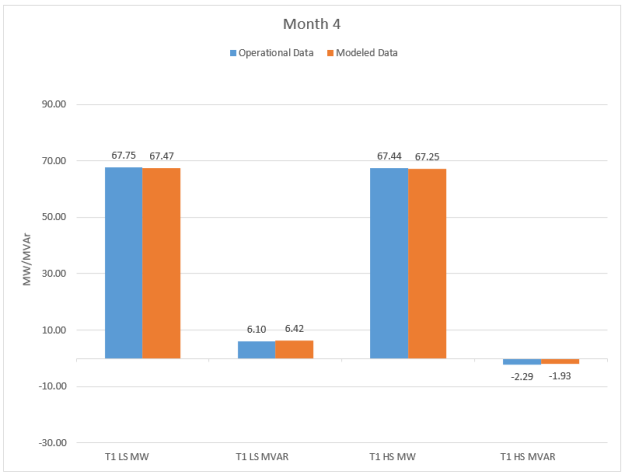

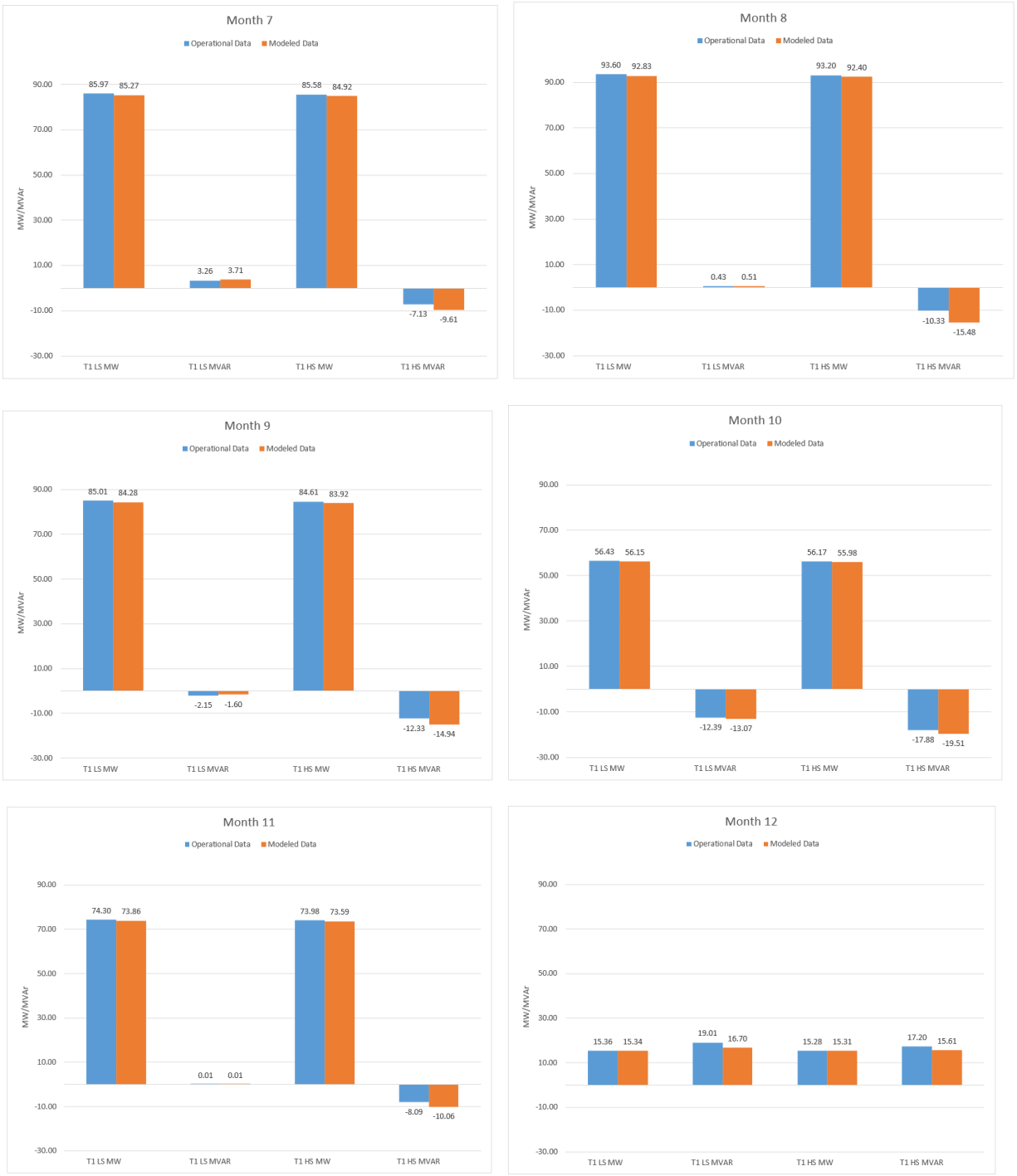

Figure 3.27 Texas Wind Farm Modeled v. Operational Active & Reactive Power Comparison

An additional check was performed on the WTG terminal voltage by comparing the calculated values from the excel tool to the historical SCADA data from the Texas wind farm. As opposed to monthly graphs, an annual graph is provided here for better visualization of the WTG modeled

and historical field data. On average the operational WTG terminal voltage was 1.01% lower than the predicted WTG terminal voltage.

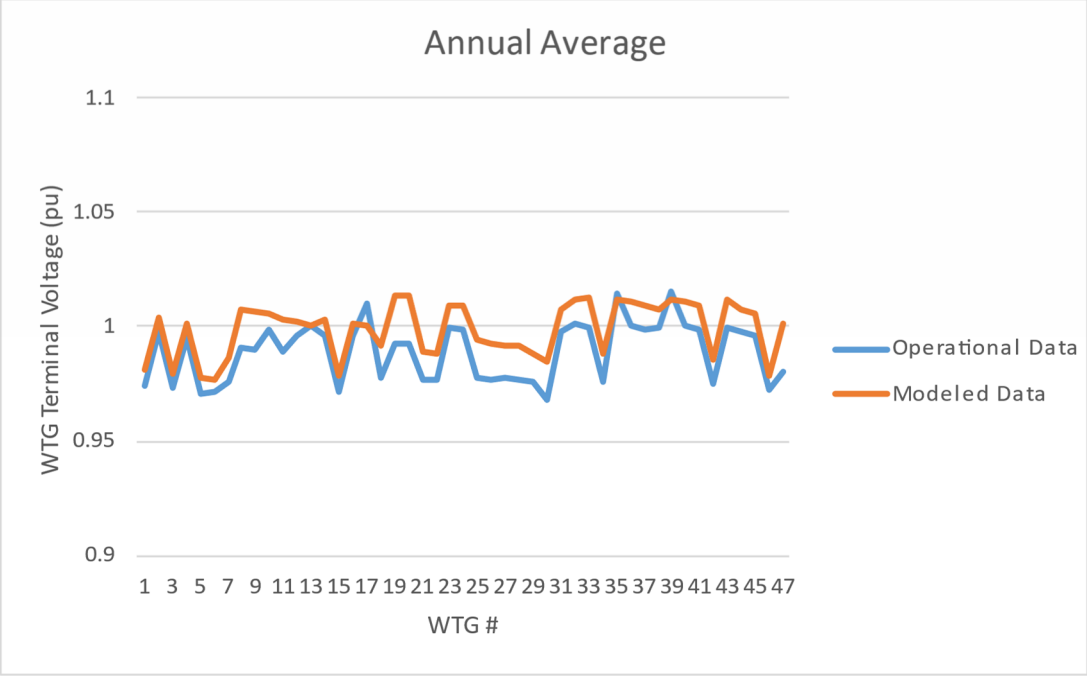

Figure 3.28 Texas Wind Farm Modeled v. Operational Voltage Magnitude Comparison

Chapter 4

4.0 Case Studies & Results

This chapter will start with a discussion on the case study setup for evaluating the base case and alternate cases for the Texas wind farm. The analysis is centered around reducing active power losses while still delivering FERC required reactive power to the POI. Alternative case studies that differ from actual plant design and operation are presented to review plant performance. Finally, a more detailed review of the optimal options is presented.

4.1 Case Study Setup

To evaluate different design and operating considerations for the Texas wind farm, data from the operating wind farm was gathered from 09/19/21 at midnight until 09/18/22 at 11PM. There were some simplifications made on the native SCADA data to make the analysis feasible. First, averaged hourly data was used as opposed to native SCADA data every second. Next, each hour of data was then categorized into 60 discrete categories based on the average WTG active and reactive power outputs. The table below shows the buckets and number assignments for each of these ranges.

Assigned numbers for each category

		Real Power					
		-1% to 0%	0% to 20%	20% to 40%	40% to 60%	60% to 80%	80% to 100%
Reactive Power	-80% to -100%	1	11	21	31	41	51
	-60% to -80%	2	12	22	32	42	52
	-40% to -60%	3	13	23	33	43	53
	-20% to -40%	4	14	24	34	44	54
	0% to -20%	5	15	25	35	45	55
	0% to 20%	6	16	26	36	46	56
	20% o 40%	7	17	27	37	47	57
	40% to 60%	8	18	28	38	48	58
	60% to 80%	9	19	29	39	49	59
	80% to 100%	10	20	30	40	50	60

Table 4.1 Category Number Assignments

After categorizing the data as described in the section above, the total number of hours the plant operated within each category from 09/19/21 to 09/18/22 was summed and converted into a percentage of overall operating time as shown in the table below.

Number of hours in each category

		Real Power					
		-1% to 0%	0% to 20%	20% to 40%	40% to 60%	60% to 80%	80% to 100%
Reactive Power	-80% to -100%	0%	0%	0%	0%	0%	0%
	-60% to -80%	0%	0%	0%	0%	0%	0%
	-40% to -60%	1%	3%	2%	1%	0%	0%
	-20% to -40%	2%	8%	7%	3%	1%	1%
	0% to -20%	4%	14%	8%	5%	3%	1%
	0% to 20%	1%	4%	2%	4%	6%	4%
	20% o 40%	0%	1%	0%	0%	2%	7%
	40% to 60%	0%	0%	0%	0%	0%	5%
	60% to 80%	0%	0%	0%	0%	0%	1%
	80% to 100%	0%	0%	0%	0%	0%	0%

Table 4.2 Category Percentage Assignments

The percentages in each bin are used to evaluate each of the cases for plant performance under varying design and operational setups. Each bin has a range for both active and reactive power. To determine a MW loss and reactive power at POI value for each bin, the Excel tool is executed at the lower active power range and lower reactive power range, lower active power range and upper reactive power range, upper active power range and lower reactive power range, and upper active power range and upper reactive power range. Once those scenarios are modeled the results are average to arrive at a number for the respective category. This allows some simplification of the modeling to prevent running the model each hour for the entire year while also still providing relevant data about how the plant was operating over the year.

Additionally, the Texas wind farm includes a shunt capacitor bank located at the 34.5kV MV bus with x3, 13.5 MVAr stages. The capacitor banks are part of the AVR control loop but not directly part of the voltage droop for VAR control at the POI. The capacitor bank logic is setup to close in a capacitor bank stage when the net WTG MVAr output exceeds 17 MVAr for more than 7 minutes. This continues sequentially for each capacitor bank as reactive power demand increases.

Alternatively, if the WTG output is -5MVAr for more than 7 minutes, a capacitor bank will be removed from service, if one is currently engaged. The capacitor banks are energized as needed in a round robin sequence to even out operational use. Given this logic, no capacitor banks are in service for any of the leading scenarios. For lagging scenarios, capacitor banks are considered when using the tool as noted in the table below.

(1)	(2)
WTG MVAr Output	Cap Bank Contribution (pu)
0%	0
20%	0
40%	0.135
60%	0.27
80%	0.405
100%	0.405

Table 4.3 Capacitor Bank Logic

In Figure 4.3, Column 1 is the MVAr output scenario for which capacitor banks would be closed in and are considered in the base case and alternative cases analyzed below. Column 2 includes the cap bank contribution from the shunt devices for each respective stage.

4.1.1 Base Case

The base case is performed and ran through the Excel tool and is used to set a baseline for current site design and operation. The substation MPT includes an OLTC regulating the MV bus to 34.5kV. The capacitor banks close in as per the logic in section 4.1. To perform the analysis, 77 load flow scenarios are ran through the Excel tool to arrive at the MW losses and POI VARs for each scenario as shown in the table below. Note the scenarios with the letters "DNC" represent scenarios where the Newton-Raphson did not converge. These points of non-convergence are not valid operating points for the plant and there are no hours in these categories recorded, hence it does not influence the analysis.

		Real Power						
		-1%	0%	20%	40%	60%	80%	100%
Reactive Power	-100%	1.16	1.15	1.46	2.37	3.85	7.85	DNC
	-80%	0.71	0.71	1.01	1.89	3.36	5.35	DNC
	-60%	0.39	0.39	0.66	1.50	2.92	4.90	7.84
	-40%	0.16	0.16	0.43	1.24	2.58	4.49	7.24
	-20%	0.04	0.04	0.30	1.08	2.37	4.23	6.73
	0%	0.01	0.01	0.26	1.01	2.25	4.02	6.35
	20%	0.07	0.07	0.32	1.03	2.22	3.92	6.04
	40%	0.11	0.26	0.36	1.14	2.25	3.84	5.94
	60%	0.15	0.51	0.39	1.32	2.34	3.80	5.74
	80%	0.20	0.82	0.43	1.57	2.53	3.92	5.67
	100%	0.36	1.13	0.58	1.85	2.76	4.09	5.78

Table 4.4 Base Case Plant MW Losses

Next, based on the percentage of plant operating times in each category per Table 4.2, the MWh losses for each category are calculated out in the table below. In addition, the total MWh electrical losses for the year are provided.

		Real Power					
		-1% to 0%	0% to 20%	20% to 40%	40% to 60%	60% to 80%	80% to 100%
Reactive Power	-80% to -100%	-	-	3.95	3.36	-	-
	-60% to -80%	-	14.63	26.72	45.36	-	-
	-40% to -60%	14.53	106.76	163.26	157.17	122.31	14.36
	-20% to -40%	13.84	161.03	442.08	411.26	284.74	253.03
	0% to -20%	7.81	183.38	463.37	736.91	789.28	544.59
	0% to 20%	4.35	52.16	111.60	596.35	1,613.05	1,628.14
	20% o 40%	3.45	17.82	23.47	17.56	520.21	2,820.14
	40% to 60%	4.53	13.81	4.71	18.62	46.65	2,120.36
	60% to 80%	-	5.68	3.27	15.93	44.30	213.23
	80% to 100%	-	1.74	-	-	-	28.54
						Total =	**14,893.43**

Table 4.5 Base Case Plant MWh Losses

From the analysis above, 1489.43MWh is the total MWh baseline loss for the Texas wind farm in its current operating state. This number will have some variance by year especially dependent on wind speed, grid conditions, and equipment age where total MWh losses may go up or down. The following cases will use this baseline loss as a reference for assessing proposed design and operation methods to reduce losses and this relative magnitude of baseline losses will help quantify improved or degraded plant performance.

In addition to active power electrical loss, these cases also consider reactive power contribution.

The FERC 827 reactive power requirement for wind and solar intermittent renewable resources is to provide at all continuous operating output points at least 0.95 lead/lag power factor control capability at the POI. The letters "DNC" represent scenarios where the Newton-Raphson did not converge and same as the calculated MW loss values this does not influence the analysis as these are not valid operating points. The MVAr values at the POI are provided below for the plant with positive values representing lagging reactive power flow (e.g. towards the grid) and negative values representing leading reactive power flow (e.g. towards the plant).

		Net Real Power						
		-1%	0%	20%	40%	60%	80%	100%
Net Reactive Power	-100%	-72.82	-72.79	-76.75	-88.10	-107.17	-162.54	DNC
	-80%	-55.34	-55.32	-58.86	-69.44	-87.80	-114.52	DNC
	-60%	-39.05	-39.04	-41.97	-51.68	-68.71	-94.47	-135.72
	-40%	-23.45	-23.44	-26.33	-35.21	-50.72	-74.61	-111.43
	-20%	-9.14	-9.13	-11.70	-19.73	-33.97	-55.97	-88.63
	0%	4.03	4.04	1.77	-5.41	-18.17	-38.12	-67.76
	20%	15.68	15.69	13.95	7.60	-3.54	-21.32	-28.52
	40%	39.74	39.74	37.90	32.26	22.74	9.07	-10.50
	60%	62.61	62.62	60.94	55.76	47.04	34.55	17.93
	80%	84.15	84.16	82.62	77.83	69.75	46.17	42.97
	100%	93.99	94.00	92.54	87.93	80.14	57.32	54.37

Table 4.6 Base Case Plant POI MVAr

Table 4.6 is provided to illustrate the MVAr values in each category which directly impacts the active power losses and is used to illustrate if we are meeting our PF requirements per NERC. The most difficult scenario to achieve the 0.95 power factor is the lagging scenarios, where the plant is exporting VARs to the grid, and at high active power outputs due to increased VAR drop across cables and transformers and the associated higher voltage at the WTG terminals required to push the reactive power. This results in the 100% active and 100% reactive power output scenario being the most difficult scenario to achieve the 0.95 power factor requirements. Therefore, this case is used as a reference check that under the alternative design or operating case conditions, the plant is still capable of complying with the requirements. For the baseline case 1 the plant provides 54.37MVAr which results in a power factor of 0.943 for the scenario and complies with FERC 827.

4.1.2 Alternative Case 1

Alternative Case 1 is the same as the base case with the exception of the removal of the capacitor banks. This case was not completely modeled but rather just the 100% active power and 100% reactive power scenarios were performed. This resulted in a MW loss of 6.103MWs (higher than the base case losses for the same case due to 34.5kV bus voltage not being raised as high) and a POI VAR export of 16.15MVAr. This case is used to illustrate that the removal of the capacitor banks is not a viable solution in and of itself to reduce losses because it will fail to comply with FERC Order 827 with a power factor of 0.995.

4.1.3 Alternative Case 2

Alternative case 2 is the same as the base case except for changing the substation MPT OLTC to regulate the MV bus to 36kV for steady-state operation. Running this tap changer adjustment through the Excel tool for the 77 scenarios results in the losses shown in Table 4.7.

		Active Power						
		-1%	0%	20%	40%	60%	80%	100%
Reactive Power	-100%	0.980	0.978	1.267	2.066	3.853	7.847	DNC
	-80%	0.587	0.586	0.859	1.639	3.036	5.350	DNC
	-60%	0.329	0.328	0.563	1.376	2.638	4.482	7.855
	-40%	0.130	0.129	0.383	1.132	2.419	4.253	6.984
	-20%	0.030	0.029	0.275	1.006	2.208	3.941	6.194
	0%	0.008	0.007	0.245	0.952	2.122	3.804	6.023
	20%	0.064	0.063	0.293	0.980	2.121	3.726	5.870
	40%	0.241	0.241	0.454	1.099	2.175	3.698	5.697
	60%	0.508	0.508	0.709	1.319	2.342	3.781	5.649
	80%	0.822	0.821	1.007	1.574	2.526	3.880	5.670
	100%	1.127	1.126	1.302	1.847	2.763	4.065	5.782

Table 4.7 Alternative Case 2 Plant MW Losses

Converting these loss values to annual energy loss for each category results in the MWh losses shown in table 4.8.

		Real Power					
		-1% to 0%	0% to 20%	20% to 40%	40% to 60%	60% to 80%	80% to 100%
Reactive Power	-80% to -100%	-	-	3.42	3.11	-	-
	-60% to -80%	-	12.33	23.43	40.77	-	-
	-40% to -60%	12.09	91.40	146.95	144.24	113.26	13.83
	-20% to -40%	11.28	143.08	406.10	382.97	267.00	238.20
	0% to -20%	6.03	169.31	435.44	691.53	740.17	509.36
	0% to 20%	3.80	47.89	105.05	565.03	1,529.59	1,555.17
	20% o 40%	4.11	18.50	23.21	16.83	498.42	2,712.49
	40% to 60%	6.59	17.38	5.25	18.31	45.74	2,064.84
	60% to 80%	-	8.04	4.05	15.93	44.10	211.53
	80% to 100%	-	2.50	-	-	-	28.44
						Total =	**14,158.09**

Table 4.8 Alternative Case 2 Plant MWh Losses

The total annual MWh losses for alternative case 2 results in 735.34MWh less loss compared to the base case. The reactive power flow for alternative case 2 is shown in Table 4.9.

		Net Real Power						
		-1%	0%	20%	40%	60%	80%	100%
Net Reactive Power	-100%	-68.85	-68.82	-72.68	-82.53	-107.19	-162.53	DNC
	-80%	-52.19	-52.16	-55.65	-65.09	-83.12	-114.54	DNC
	-60%	-37.36	-37.34	-39.74	-49.77	-65.19	-89.28	-135.94
	-40%	-22.36	-22.35	-25.29	-33.91	-49.34	-72.46	-116.56
	-20%	-8.54	-8.53	-11.24	-19.35	-33.31	-54.54	-84.51
	0%	4.65	4.66	2.17	-5.39	-18.49	-38.27	-66.63
	20%	17.10	17.11	14.83	7.86	-4.28	-22.63	-48.88
	40%	40.60	40.60	38.80	32.94	22.75	7.32	-15.02
	60%	62.61	62.62	60.94	55.76	47.03	34.41	16.03
	80%	84.15	84.16	82.62	77.83	69.75	58.22	42.96
	100%	93.99	94.00	92.54	87.93	80.14	69.05	54.38

Table 4.9 Alternative Case 2 Plant POI MVAr

With the adjustment to the MPT OLTC there is more impact to the scenarios with leading reactive power where the voltage is being raised even higher to regulate the MV bus. Whereas with the lagging scenarios, the MV bus is inherently raised with the increase in reactive power export, so the tap adjustment impact is limited to an extent. Given this the worst-case lagging scenario provides 54.38, very similar to the base case, and has a satisfactory power factor at 0.943.

4.1.4 Alternative Case 3

Alternate case 3 is the same as the base case with the exception of having the shunt capacitor banks on the MV bus relocated to the HV bus. The same control logic for closing in the capacitor banks based on WTG MVAr flow is deployed for modeling with the Excel tool. The calculated MW losses for each category in this case are provided in Table 4.10.

		Active Power						
		-1%	0%	20%	40%	60%	80%	100%
Reactive Power	-100%	1.16	1.15	1.46	2.37	3.85	7.85	DNC
	-80%	0.71	0.71	1.01	1.89	3.36	5.35	DNC
	-60%	0.39	0.39	0.66	1.50	2.92	4.90	7.84
	-40%	0.16	0.16	0.43	1.24	2.58	4.49	7.24
	-20%	0.04	0.04	0.30	1.08	2.37	4.23	6.73
	0%	0.01	0.01	0.26	1.01	2.25	4.02	6.35
	20%	0.07	0.07	0.32	1.03	2.22	3.92	6.04
	40%	0.23	0.23	0.46	1.15	2.28	3.91	6.05
	60%	0.43	0.43	0.64	1.29	2.39	3.96	6.02
	80%	0.68	0.68	0.88	1.50	2.55	4.05	6.05
	100%	0.98	0.98	1.17	1.76	2.77	4.20	6.10

Table 4.10 Alternative Case 3 Plant MW Losses

Converting these loss values to annual energy loss for each operating category results in the MWh losses provided in Table 4.11.

		Real Power					
		-1% to 0%	0% to 20%	20% to 40%	40% to 60%	60% to 80%	80% to 100%
Reactive Power	-80% to -100%	-	-	3.95	3.36	-	-
	-60% to -80%	-	14.63	26.72	45.36	-	-
	-40% to -60%	14.53	106.76	163.26	157.17	122.31	14.36
	-20% to -40%	13.84	161.03	442.08	411.26	284.74	253.03
	0% to -20%	7.81	183.38	463.37	736.91	789.28	544.59
	0% to 20%	4.35	52.16	111.60	596.35	1,613.05	1,628.14
	20% o 40%	4.09	19.11	24.34	17.65	524.24	2,844.91
	40% to 60%	5.83	16.05	5.20	18.77	47.81	2,187.15
	60% to 80%	-	6.94	3.80	15.88	45.57	223.71
	80% to 100%	-	2.17	-	-	-	29.90
						Total =	**15,012.52**

Table 4.11 Alternative Case 3 Plant MWh Losses

As can be seen from Table 4.11 the plant MWh losses are higher than the base case when placing the capacitor banks on the HV bus. Intuitively it would be expected the losses for an HV bus placed capacitor bank would be less given you will have less load loss through the substation

MPT but the MV bus located cap banks will help drive the MV bus voltage up and lower current in collection system which helps support loss reduction. An important note here is that HV bus located capacitor banks would be an option for the design if the voltage drop across the collection system was causing overvoltages at the WTG terminals because the OLTC is better able to regulate to nominal MV bus voltage without capacitor banks on the bus.

		Net Real Power						
		-1%	0%	20%	40%	60%	80%	100%
Net Reactive Power	-100%	-72.82	-72.79	-76.75	-88.10	-107.17	-162.54	DNC
	-80%	-55.34	-55.32	-58.86	-69.44	-87.80	-114.52	DNC
	-60%	-39.05	-39.04	-41.97	-51.68	-68.71	-94.47	-135.72
	-40%	-23.45	-23.44	-26.33	-35.21	-50.72	-74.61	-111.43
	-20%	-9.14	-9.13	-11.70	-19.73	-33.97	-55.97	-88.63
	0%	4.03	4.04	1.77	-5.41	-18.17	-38.12	-67.76
	20%	15.68	15.69	13.95	7.60	-3.54	-21.32	-28.52
	40%	40.84	40.85	38.91	33.02	23.16	7.93	-16.00
	60%	65.88	65.89	64.06	58.45	48.97	35.33	15.12
	80%	90.44	90.45	88.72	83.36	74.31	61.31	43.92
	100%	101.06	101.07	99.45	94.32	85.65	73.22	56.65

Table 4.12 Alternative Case 3 Plant POI MVAr

The plant POI MVAr values remain nearly identical for the leading cases when compared to the base case. However, for the lagging scenarios there is an increase in MVAr available at the POI. For the worst-case scenario at max active and reactive power output the plant is able to export 56.65MVAr and achieve a satisfactory 0.940 power factor, a slight improvement from the base case.

4.1.5 Alternative Case 4

Alternative Case 4 is the same as the base case with the exception of having the substation MPT OLTC regulate the MV bus to 38kV for steady-state operation. Similar values are experienced as compared to alternative case 2 but this case pushes the voltage regulation towards the upper threshold of acceptable voltages for the MV bus. Running this tap changer adjust through the Excel tool for the 77 scenarios results in the losses provided in Table 4.13.

		Active Power						
		-1%	0%	20%	40%	60%	80%	100%
Reactive Power	-100%	0.870	0.868	1.146	2.066	3.853	7.840	DNC
	-80%	0.456	0.455	0.711	1.402	2.844	5.347	DNC
	-60%	0.233	0.232	0.426	1.175	2.380	4.237	7.805
	-40%	0.057	0.056	0.291	1.008	2.182	3.760	6.112
	-20%	0.005	0.004	0.219	0.909	2.047	3.604	5.606
	0%	0.002	0.002	0.222	0.877	1.979	3.500	5.555
	20%	0.060	0.059	0.275	0.910	1.977	3.456	5.431
	40%	0.225	0.225	0.429	1.038	2.057	3.483	5.376
	60%	0.476	0.475	0.669	1.252	2.226	3.595	5.364
	80%	0.809	0.809	0.992	1.548	2.480	3.789	5.464
	100%	1.127	1.126	1.302	1.847	2.753	4.012	5.659

Table 4.13 Alternative Case 4 Plant MW Losses

Converting these loss values to annual energy loss for each operating category results in the MWh losses provided in Table 4.14.

		Active Power					
		-1% to 0%	0% to 20%	20% to 40%	40% to 60%	60% to 80%	80% to 100%
Reactive Power	-80% to -100%	-	-	3.12	2.98	-	-
	-60% to -80%	-	9.63	19.61	36.61	-	-
	-40% to -60%	7.64	65.45	123.33	128.60	103.14	12.85
	-20% to -40%	4.35	99.79	352.25	347.88	241.40	212.67
	0% to -20%	1.03	135.70	390.96	639.07	682.18	466.06
	0% to 20%	3.27	43.82	97.09	525.44	1,417.69	1,436.64
	20% o 40%	3.84	17.38	21.78	15.79	466.64	2,534.79
	40% to 60%	6.17	16.35	4.97	17.35	43.32	1,954.46
	60% to 80%	-	7.78	3.93	15.41	42.55	202.97
	80% to 100%	-	2.48	-	-	-	27.75
						Total =	**13,015.97**

Table 4.14 Alternative Case 4 Plant MWh Losses

The results show a 1,877MWh improvement over the base case annual electric power losses. The increased voltage regulation point results in less current running through the underground cables and resultingly less losses. The below table shows the resultant POI MVAr values for this case.

		Net Active Power						
		-1%	0%	20%	40%	60%	80%	100%
Net Reactive Power	-100%	-66.10	-66.07	-69.86	-82.53	-107.19	-162.44	DNC
	-80%	-48.45	-48.43	-51.84	-59.99	-79.88	-114.49	DNC
	-60%	-34.29	-34.28	-35.80	-45.63	-60.91	-85.80	-135.04
	-40%	-19.53	-19.51	-22.42	-31.44	-45.96	-66.16	-94.15
	-20%	-7.24	-7.23	-9.34	-17.68	-31.40	-50.97	-76.61
	0%	5.50	5.51	2.98	-4.41	-17.36	-36.08	-63.00
	20%	17.70	17.71	15.35	8.32	-3.89	-21.69	-46.72
	40%	41.34	41.34	39.28	32.97	22.11	6.09	-16.15
	60%	63.58	63.59	61.78	56.21	46.64	32.51	12.76
	80%	84.45	84.46	82.89	78.02	69.65	57.35	39.82
	100%	93.99	94.00	92.54	87.93	80.13	68.58	52.54

Table 4.15 Alternative Case 4 Plant POI MVAr

The worst-case maximum active and reactive power output to the grid results in 52.45MVAr for this alternative case with an associated 0.947 power factor. This is slightly worse than the reactive power provided in the base case by approximately 2 MVAr.

4.1.6 Alternative Case 5

Alternative case 5 is the same as the base case with the exception of replacing the underground collection cables with overhead ACSR conductors and adding in an additional 13.5MVAr step at the MV bus. The additional 13.5MVAr step is required because without the added VArs the site is unable to satisfy the 0.95 lagging power factor requirement for maximum active and reactive power output scenario. The increased inductive reactance and lower capacitive reactance of the overhead conductors compared to the underground cables drives the need to add an extra capacitor bank stage for analysis. Underground TRXLPE cables are used in the original design and this case replaces the collection system with a 1590 aluminum conductor steel reinforced (ACSR) "Falcon" conductor. Lengths between all of the WTGs remain the same and a single conductor per phase is considered.

A comparative table of the resistance, reactance and capacitance between the underground cables and overhead Falcon conductor is provided in the table below for reference.

Cable Type	Positive Sequence Resistance R+ (ohms/kft)	Positive Sequence Reactance X+ (ohms/kft)	Positive Sequence Capacitance C+
1/0 AWG	0.238	0.054	0.039
4/0 AWG	0.114	0.048	0.049
500 kcmil	0.050	0.043	0.063
750 kcmil	0.037	0.041	0.073
1000 kcmil	0.027	0.039	0.083
1250 kcmil	0.023	0.037	0.090
1590 ACSR "Falcon"	0.012	0.142	0.003

Table 4.16 Underground and Overhead Impedances

With the overhead ACSR conductor, the associated power loss values for each category for this case are provided in Table 4.17.

		Active Power						
		-1%	0%	20%	40%	60%	80%	100%
Reactive Power	-100%	0.87018152	0.8686	1.1149589	1.69896075	3.41524552	DNC	DNC
	-80%	0.54510032	0.5441	0.7283435	1.37395643	2.47861149	4.98270172	DNC
	-60%	0.29789649	0.2972	0.5019909	1.09522428	2.14765379	3.71425408	DNC
	-40%	0.12975972	0.1292	0.3196364	0.90002504	1.8756433	3.3563683	5.1300865
	-20%	0.0351395	0.0347	0.2138622	0.76003526	1.69405967	3.06078041	5.04743297
	0%	0.00606929	0.0057	0.1750213	0.68620999	1.56643613	2.87031584	4.68021251
	20%	0.04520777	0.044790856	0.2045672	0.67988083	1.51022466	2.72720995	4.45163868
	40%	0.17566714	0.175250833	0.3198644	0.75819675	1.50696527	2.59024098	4.11743932
	60%	0.34363127	0.343188812	0.4754638	0.87773683	1.56229189	2.55789509	3.91893239
	80%	0.63057332	0.630116025	0.7483189	1.10983448	1.72269594	2.60690555	3.79730997
	100%	0.82899581	0.82847589	0.9411927	1.28856073	1.87744866	2.72552461	3.86067215

Table 4.17 Alternative Case 5 Plant MW Losses

Converting these loss values to annual energy loss for each operating category results in the MWh losses provided in Table 4.18.

		Active Power					
		-1% to 0%	0% to 20%	20% to 40%	40% to 60%	60% to 80%	80% to 100%
Reactive Power	-80% to -100%	-	-	2.88	2.63	-	-
	-60% to -80%	-	10.94	19.53	33.30	-	-
	-40% to -60%	11.27	81.26	119.79	114.74	91.10	7.16
	-20% to -40%	11.67	122.11	318.46	296.03	207.96	184.95
	0% to -20%	6.62	130.41	322.40	517.67	563.42	399.55
	0% to 20%	2.71	33.80	74.24	406.54	1,127.02	1,179.36
	20% o 40%	2.97	13.10	16.12	11.76	354.45	1,983.45
	40% to 60%	4.57	11.94	3.57	12.42	31.33	1,446.22
	60% to 80%	-	5.80	2.83	10.82	29.74	143.56
	80% to 100%	-	1.85	-	-	-	19.05
						Total =	**10,505.05**

Table 4.18 Alternative Case 5 Plant MWh Losses

The total annual MWh losses for this case are 4,388.38MWh. Changing the cables out with ACSR conductors provides the largest savings in MWh for any of the cases evaluated. The plant POI MVAr values are provided in Table 4.19.

		Net Active Power						
		-1%	0%	20%	40%	60%	80%	100%
Net Reactive Power	-100%	-79.71	-79.68	-84.49	-95.24	-129.75	DNC	DNC
	-80%	-61.33	-61.31	-64.56	-76.70	-98.04	-148.28	DNC
	-60%	-44.10	-44.09	-47.79	-58.59	-78.44	-109.50	DNC
	-40%	-28.17	-28.16	-31.48	-41.73	-59.75	-88.35	-121.40
	-20%	-13.48	-13.47	-16.47	-25.75	-42.41	-68.36	-108.32
	0%	0.08	0.08	-2.63	-11.00	-26.08	-49.89	-85.79
	20%	12.30	12.31	9.87	2.53	-10.79	-32.49	-65.28
	40%	35.67	35.67	33.57	27.19	16.30	-0.27	-26.51
	60%	58.40	58.41	56.50	50.68	40.77	26.38	6.72
	80%	90.59	90.60	88.92	83.74	74.96	62.28	45.25
	100%	100.03	100.04	98.43	93.44	84.99	72.80	56.53

Table 4.19 Alternative Case 5 Plant POI MVAr

The MVAr provided for the worst-case maximum active and reactive power outputs results in 56.63MVAr provided to the POI at a 0.941 power factor. This is an improvement from the base case VArs provided to the POI and is compliant with FERC requirements but this case does require the addition of another cap bank stage that does not currently exist in the field. Without this additional capacitor bank the plant can only deliver 44.24MVAr to the POI at a 0.962 power factor. Once this was noticed the additional capacitor bank was added into the analysis to make it more similar to the other cases, so enough reactive power would still have to be provided by the plant.

4.1.7 Alternative Case 6

In alternative case 6 it is the same as the base case except for the substation MPT OLTC regulation strategy. For leading scenarios where the WTGs are absorbing reactive power the MV bus is regulated to 38kV. For lagging scenarios where the WTGs are supplying reactive power to the grid the MV bus is regulated to 36kV. This strategy is built around the concept that reactive power flows in the direction of high voltage magnitude to low voltage magnitude. With that,

raising the voltage to 38kV for the leading scenarios will help raise the voltage seen at the WTGs during stead-state operation and if there is a low-voltage ride-through (LVRT) event the WTG will stand a better chance of riding through. The higher voltage results in lower current output from the WTGs which results in lower annual energy loss, as well as provides support in cable ampacity calculations for sizing the underground cables.

For the lagging scenario, the MPT OLTC regulation mechanism is set to regulate the voltage to 36kV. This is selected because as the WTGs supply reactive power to the grid, they will drive the voltage at the MV bus up. Most MV bus equipment is rated continuously up to 38kV so to not exceed this for steady-state operation the regulation point for this case is lowered slightly to provide headroom for voltage swells for high voltage ride-through (HVRT) events.

The MW losses for each scenario are presented in Table 4.20.

		Active Power						
		-1%	0%	20%	40%	60%	80%	100%
Reactive Power	-100%	0.870	0.868	1.146	2.066	3.853	7.840	DNC
	-80%	0.456	0.455	0.711	1.402	2.844	5.347	DNC
	-60%	0.233	0.232	0.426	1.175	2.380	4.237	7.805
	-40%	0.057	0.056	0.291	1.008	2.182	3.760	6.112
	-20%	0.005	0.004	0.219	0.909	2.047	3.604	5.606
	0%	0.002	0.002	0.222	0.877	1.979	3.500	5.555
	20%	0.064	0.063	0.293	0.980	2.121	3.726	5.870
	40%	0.241	0.241	0.454	1.099	2.175	3.698	5.697
	60%	0.508	0.508	0.709	1.319	2.342	3.781	5.649
	80%	0.822	0.821	1.007	1.574	2.526	3.880	5.670
	100%	1.127	1.126	1.302	1.847	2.763	4.065	5.782

Table 4.20 Alternative Case 6 Plant MW Losses

The MWh losses for this case are presented in Table 4.21.

		Active Power					
		-1% to 0%	0% to 20%	20% to 40%	40% to 60%	60% to 80%	80% to 100%
Reactive Power	-80% to -100%	-	-	3.12	2.98	-	-
	-60% to -80%	-	9.63	19.61	36.61	-	-
	-40% to -60%	7.64	65.45	123.33	128.60	103.14	12.85
	-20% to -40%	4.35	99.79	352.25	347.88	241.40	212.67
	0% to -20%	1.03	135.70	390.96	639.07	682.18	466.06
	0% to 20%	3.49	45.61	100.84	545.02	1,471.47	1,493.37
	20% o 40%	4.11	18.50	23.21	16.83	498.42	2,712.49
	40% to 60%	6.59	17.38	5.25	18.31	45.74	2,064.84
	60% to 80%	-	8.04	4.05	15.93	44.10	211.53
	80% to 100%	-	2.50	-	-	-	28.44
						Total =	**13,492.38**

Table 4.21 Alternative Case 6 Plant MWh Losses

The resulting annual energy loss is 1,401.05MWh less than the original base case. Additionally, the reactive power at the POI for this regulation case is provided in Table 4.22.

		Net Active Power						
		-1%	0%	20%	40%	60%	80%	100%
Net Reactive Power	-100%	-66.10	-66.07	-69.86	-82.53	-107.19	-162.44	DNC
	-80%	-48.45	-48.43	-51.84	-59.99	-79.88	-114.49	DNC
	-60%	-34.29	-34.28	-35.80	-45.63	-60.91	-85.80	-135.04
	-40%	-19.53	-19.51	-22.42	-31.44	-45.96	-66.16	-94.15
	-20%	-7.24	-7.23	-9.34	-17.68	-31.40	-50.97	-76.61
	0%	5.50	5.51	2.98	-4.41	-17.36	-36.08	-63.00
	20%	17.10	17.11	14.83	7.86	-4.28	-22.63	-48.88
	40%	40.60	40.60	38.80	32.94	22.75	7.32	-15.02
	60%	62.61	62.62	60.94	55.76	47.03	34.41	16.03
	80%	84.15	84.16	82.62	77.83	69.75	58.22	42.96
	100%	93.99	94.00	92.54	87.93	80.14	69.05	54.38

Table 4.22 Alternative Case 6 Plant POI MVAr

The resulting POI MVAr for the worst-case maximum active and reactive power output will be the same as alternative case 2 which provides 54.38 MVAr, very similar to the base case, and has a satisfactory power factor at 0.943.

4.2 Preferred Solutions

The Texas wind farm was built in 2019 and the above cases review annual energy electrical losses due to current design in the base case and alternative cases with varied methods to reduce active power losses while still meeting reactive power reliability requirements. To help quantify some of the economic improvement from the annual energy electrical loss, the below data from Lawrence Berkley National Laboratory is used as a reference point. It includes data from 2021 which matches the time period of the SCADA data. This includes the average wholesale electricity market price for energy of known windfarms in ERCOT and while not a perfect method given varying nodal price variations across the ERCOT market, it provides a relative metric for range of magnitude impact considering the year over year pricing in 2022 dollars. The average wholesale electricity LMP received in 2021 was $33.85/MWh.

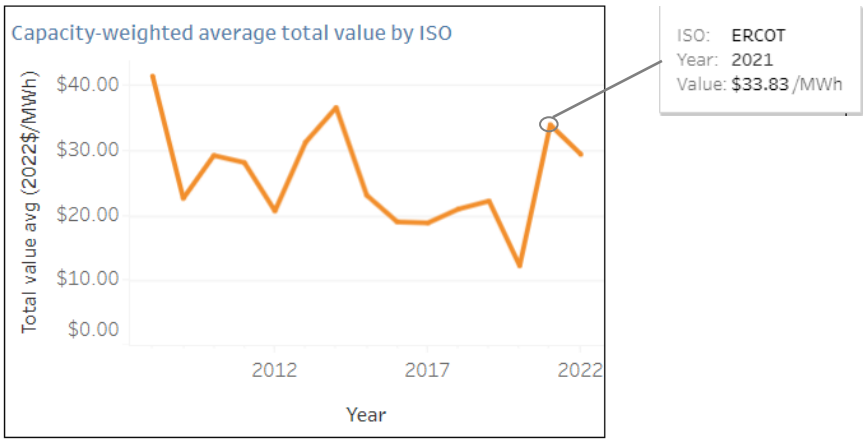

Source: Wind Energy Market Value, [67]

Figure 4.1 2021 ERCOT Capacity-Weighted Average Wind Farm LMP

The price quantification is used to put into relative perspective the economic benefit of options to minimize annual electrical energy loss for the plant. It is important to note there are other factors that are not considered that make each MWh even more valuable such as the PTCs, RECs and PPAs. Two preferred solutions are provided below to be considered for future wind farm design and operational setup. Also, the Texas wind farm had a poor capacity factor for the year under analysis due to a variety of factors, and if this capacity factor is improved to a higher industry standard of around 40% the financial benefit of the below recommendations will grow accordingly.

A preferred solution from a design perspective is to use overhead ACSR conductors for loop-fed connections between utility scale WTGs. The project is compliant with FERC and ERCOT reactive power study requirements as shown with the Excel tool using the Newton-Raphson load flow equations. The overhead cables have lower higher inductive reactance and lower capacitive reactance which will likely cause the need for additional minor shunt capacitors for the project. Even with the addition of the shunt capacitor bank stage, the overhead ACSR conductors are preferred because this provides a large improvement in annual electrical energy loss for the plant. The plant design results in a savings of 4,388.38MWh each year in operation. When considering

Berkley Lab's ERCOT LMP pricing this would equate to an annual savings of $148,546.60 in energy alone.

Additionally, the cost for materials and labor on an overhead distribution voltage line is typically less than that of an underground distribution voltage line. Another consideration is underground distribution lines are subject to failures, especially cable insulation, terminations and splices, similar to how overhead lines are subject to failures from things such as animals, lightening, trees. The reliability of the service selected should be specific to the geographical area and should be considered as one of the driving inputs in determining if keeping the conductors above ground is acceptable. Another consideration is the physical perspective of having above ground lines ran to connect distributed IBRs on a utility-scale project that may be miles apart from each other and obtaining landowner and authority having jurisdiction (AHJ) approval to do so.

A preferred solution from an operating standpoint would be to regulate the MV bus to an off-nominal voltage based on reactive power flow direction. This is illustrated in alternative case 6 where the low side of the substation MPT is regulated with the OLTC to 36kV for lagging reactive power flow and to 38kV for leading reactive power flow. This regulation method reduces the active power losses throughout the wind farm by decreasing the current flowing throughout the system, while also providing improved performance of the plant for LVRT and leaves headroom for HVRT. This can be modeled at the early stage of the utility scale renewable project to show estimated losses and it can be tuned for operational projects based on SCADA data and actual grid conditions to further improvement. From the Excel tool running Newton-Raphson load flow, it is shown that the annual energy losses for this regulation method results in an annual electrical energy loss savings of 1,401.05MWh over the base case. Referring again to Berkley Lab's ERCOT LMP pricing this equates to an annual savings for the facility of $47,397.45 in energy alone. The big benefit to this solution is it can be done with just updates to the controls and no change to any physical equipment at the plant.

Chapter 5

5.0 Conclusions & Future Work

This thesis was focused on two central topics with the first being the creation of an Excel based tool to perform complete linearized Newton-Raphson load flow for evaluating wind farm power flow for economic impact, and the second was performing a specific evaluation based on an operational Texas wind farm with a review of alternative design and operational techniques. The results of this work result in an Excel tool that can be used to perform future study work and some considerations for engineers performing power flow studies for wind farms. Overhead conductors have been used for decades throughout the US distribution system but are not typically utilized for wind plant design and some of the economic benefits of doing so are displayed in this paper. Additionally, a new method for regulating wind farm substation MV bus with the MPT OLTC to two separate setpoints dependent on reactive power flow direction was provided along with the economic benefit.

Future work can include a detailed cost breakdown of overhead verse underground cables along with the reliability associated with each technology. Future work could also include the impacts and effects of harmonic currents on the losses which was a topic discussed in [51]. Additionally, long time-horizon based research into continuous higher voltage on equipment and any deterioration of insulation properties. Further research into bundled conductors/phase and varying conductor material for the collection system of a wind farm would be valuable research. The design and implementation of the OLTC controller at an operational site for future works would be a valuable case study to prove out more complex voltage control points. The use of the Excel tool to directly read-in SCADA data at an operational facility to tune the model as a digital twin and make changes to the controller target voltage setpoint based on expected grid conditions would be another research area of interest. As goals in the US for net zero continue to increase

there will be a continuous rise in utility-scale facilities built and a focus on designing and operating these facilities in a safe, reliable, and economic manner will help us achieve these goals quicker.

Bibliography

[1] M. D. Smith, Newton-Raphson Technique, https://web.mit.edu/10.001/Web/Course_Notes/NLAE/node6.html.

[2] Q. Kong, T. Siauw, and A. Bayen, Python Numerical Methods, https://pythonnumericalmethods.berkeley.edu/notebooks/chapter19.04-Newton-Raphson Method.html.

[3] "Intermittent Renewable Resources," ERCOT Market Education, https://www.ercot.com/files/docs/2023/12/06/2023_12-irr.pdf.

[4] M. Albadi, "Power Flow Analysis," IntechOpen, https://www.intechopen.com/chapters/65445.

[5] K. Rhee, "Clustering Based Optimization and Automation of Utility Scale Solar Site Design," IEEE Xplore, https://ieeexplore.ieee.org/stamp/stamp.jsp?tp=&arnumber=9300981.

[6] S. A. A. Quadri, M. M. Baalbaki, A. Chacko, and M. T. Iqbal, "Design and Simulate a 500 MW Grid-Connected PV Farm for Labrador," IEEE Xplore, https://ieeexplore.ieee.org/stamp/stamp.jsp?tp=&arnumber=9795808.

[7] W. Ali et al., "Design Considerations of Stand-Alone Solar Photovoltaic Systems," IEEE Xplore, https://ieeexplore.ieee.org/stamp/stamp.jsp?tp=&arnumber=8610970.

[8] C. E. Mokhi and A. Addaim, "Optimal Design of the Cable Layout in Offshore Wind Farms using Firefly Algorithm and Minimum Spanning Tree," IEEE Xplore, https://ieeexplore.ieee.org/stamp/stamp.jsp?tp=&arnumber=9442631.

[9] Yang, XS., (2009). Firefly Algorithms for Multimodal Optimization. In Proceedings of 5th International Symposium on Stochastic Algorithms, Foundations and Applications (SAGA2009), Lecture Notes in Computer Science, October 26–28; Sapporo, Japan, pp.169-178.

[10] Yang, XS., 2010. Firefly Algorithm, Stochastic Test Functions and Design Optimisation. International Journal of Bio-inspired Computation, 2, pp.78-84.

[11] Yang, XS., 1st eds., 2014. Cuckoo Search and Firefly Algorithm, Theory and Applications. Springer International Publishing; ISBN 978-3-319-02141-6.

[12] Yang, XS., 1st eds., 2018. Nature-Inspired Algorithms and Applied Optimization. Springer International Publishing; ISBN 978-3-319-67669-2.

[13] C. E. Mokhi and A. Addaim, "Optimal Substation Location Of A Wind Farm Using Different Metaheuristic Algorithms," IEEE Xplore, https://ieeexplore.ieee.org/stamp/stamp.jsp?tp=&arnumber=9094469.

[14] Won-Sik Moon, Jae-Chul Kim, Ara Jo, and Jong-Nam Won, "Grid optimization for offshore wind farm layout and substation location," in Proc. 2014 IEEE Conference and Expo Transportation Electrification Asia-Pacific (ITEC Asia-Pacific), 2014, pp. 1–6.

[15] A. C. Pillai, J. Chick, L. Johanning, M. Khorasanchi, and V. de Laleu, "Offshore wind farm electrical cable layout optimization," Eng. Optim., vol. 47, no. 12, pp. 1689–1708, Dec. 2015.

[16] A. Wędzik, T. Siewierski, and M. Szypowski, "A new method for simultaneous optimizing of wind farm's network layout and cable crosssections by MILP optimization," Appl. Energy, vol. 182, pp. 525–538, Nov. 2016.

[17] R. Srikakulapu and V. U, "Optimal design of collector topology for offshore wind farm based on ant colony optimization approach," in Proc. 2016 IEEE International Conference on Power Electronics, Drives and Energy Systems (PEDES), 2016, pp. 1–6.

[18] H. Tahery and S. Kucuksari, "Offshore Wind Farm Collection Cable Layout Optimization through Cost Minimization," IEEE Xplore, https://ieeexplore.ieee.org/stamp/stamp.jsp?tp=&arnumber=9000348.

[19] Ling-Ling, H., Ning, C., Hongyue, Z., et al.: 'Optimization of largescale offshore wind farm electrical collection systems based on improved FCM'. Int. Conf. On Sustainable Power Generation and Supply (SUPERGEN 2012), Hangzhou,8–9 September 2012

[20] J. Li, X. Wu, W. Hu, Q. Huang, and Z. Chen, "Substation Location and Cable Connection Optimization of Onshore Wind Farms Using Minimum Spanning Tree Algorithm," IEEE Xplore, https://ieeexplore.ieee.org/stamp/stamp.jsp?tp=&arnumber=8566298.

[21] J.-A. Perez-Rua and N. A. Cutululis, "Electrical Cable Optimization in Offshore Wind Farms—A Review," IEEE Xplore, https://ieeexplore.ieee.org/document/8751957/.

[22] “BAL-003-2 – Frequency Response and Frequency Bias Setting,” NERC, https://www.nerc.com/pa/Stand/Reliability%20Standards/BAL-003-2.pdf.

[23] “VAR-002-4.1 — Generator Operation for Maintaining Network Voltage Schedules,” NERC, https://www.nerc.com/pa/Stand/Reliability%20Standards/VAR-002-4.1.pdf.

[24] T. Chakraborty et al., “Design, Implementation, and Application Guidelines of Master Power Plant Controllers in Dynamic Analysis for Grid Code Requirements,” IEEE Xplore, https://ieeexplore.ieee.org/stamp/stamp.jsp?tp=&arnumber=10215411 .

[25] “Reliability Guideline - Performance, Modeling, and Simulations of BPS Connected Battery Energy Storage Systems and Hybrid Power Plants,” NERC, https://www.nerc.com/comm/RSTC_Reliability_Guidelines/Reliability_Guideline_BESS_Hybrid_Performance_Modeling_Studies_.pdf.

[26] Y. Li, Z. Xu, J. Zhang, and K. J. I. T. o. S. E. Meng, "Variable droop voltage control for wind farm," vol. 9, no. 1, pp. 491-493, 2017.

[27] J. Kim, J.-K. Seok, E. Muljadi, and Y. C. J. I. T. o. P. E. Kang, "Adaptive Q–V scheme for the voltage control of a DFIG-based wind power plant," vol. 31, no. 5, pp. 3586-3599, 2015.

[28] D.-Y. Gau and Y.-K. Wu, “Overview of Reactive Power and Voltage Control of Offshore Wind Farms,” IEEE Xplore, https://ieeexplore.ieee.org/stamp/stamp.jsp?tp=&arnumber=9394181.

[29] C. M. Rocha-Osorio et al., “Power Control of a Doubly Fed Induction Wind Generator employing a Takagi-Sugeno Fuzzy Logic Controller,” IEEE Xplore, https://ieeexplore.ieee.org/stamp/stamp.jsp?tp=&arnumber=9065821.

[30] “Standard MOD-025-2 — Verification and Data Reporting of Generator Real and Reactive Power Capability and Synchronous Condenser Reactive Power Capability,” NERC, https://www.nerc.com/pa/Stand/Reliability%20Standards/MOD-025-2.pdf.

[31] IEEE Recommended Practice for Industrial and Commercial Power Systems Analysis. New York: Institute of Electrical and Electronics Engineers, 1998.

[32] Ward, J. B., and Hale, H. W., “Digital Computer Solution of Power Flow Problems,” AIEE Transactions, Part III—Power Apparatus and Systems, vol. 75, pp. 398–404, June 1956.

[33] Tinney, W. F., and Hart, C. E., “Power flow solution by Newton’s method,”

IEEE Transactions on Power Apparatus and Systems, vol. PAS-86, pp. 1444–1460, Nov. 1967.

[34] J. D. Glover, M. S. Sarma, and T. J. Overbye, Power System Analysis and Design. Stamford, CT: Cengage Learning, 2008.

[35] J. M. Cano, R. R. Mojumdar, and G. A. Orcajo, “Reconciling Tap-Changing Transformer Models,” IEEE Xplore, https://ieeexplore.ieee.org/stamp/stamp.jsp?tp=&arnumber=8827633.

[36] H. MA et al., Optimal Reactive Power Allocation of a Wind Farm with SVG for Voltage Stability Enhancement, https://ieeexplore.ieee.org/stamp/stamp.jsp?tp=&arnumber=10330963.

[37] Hua Yang, Haifeng Liang, Gengyin Li. A coordinated voltage control strategy for wind farm containing doubly fed induction generators [J]. Power System Technology, 2011, 35(2) : 121-126.

[37] F. Ni et al., “Optimal Control Strategy of Reactive Power and Voltage for Wind Farm Based on LinWPSO Algorithm ,” IEEE Xplore, https://ieeexplore.ieee.org/stamp/stamp.jsp?tp=&arnumber=10239582.

[38] Hua Yang, Haifeng Liang, Gengyin Li. A coordinated voltage control strategy for wind farm containing doubly fed induction generators [J]. Power System Technology, 2011, 35(2) : 121-126.

[39] B. Livadariu, G. Grigoras, F. Scarlatache, and B.-C. Neagu, “Voltage Control in Electric Networks with Wind Farms Connected Using a Scenario-Based Optimization Framework,” IEEE Xplore, https://ieeexplore.ieee.org/stamp/stamp.jsp?tp=&arnumber=10187415.

[40] M. Purlu and B. E. Turkay, “Optimal Allocation of Renewable Distributed Generations Using Heuristic Methods to Minimize Annual Energy Losses and Voltage Deviation Index,” IEEE Xplore, https://ieeexplore.ieee.org/stamp/stamp.jsp?tp=&arnumber=9718084.

[41] U. Jamil, N. Qayyum, A. Mahmood, and A. Amin, “Control Grid Strategies for Reduction of Real and Reactive Line Losses in Radial Power Distribution System,” IEEE Xplore, https://ieeexplore.ieee.org/stamp/stamp.jsp?tp=&arnumber=8940729.

[42] S. Y WANG, L. Z. ZHU, N. CHEN, et al, "A reactive power control strategy for wind farm based on hierarchical layered principle," Automation of Electric Power Systems, vol. 33, no. 13, pp. 83-87, 2009.

[43] C. F. WANG, J. LIANG, L. ZHANG, et al, "Reactive power and voltage control strategy for wind farm based on STATCOM," Proceedings of the CSEE, vol. 30, no. 25, pp. 23-28, 2010.

[44] Y. Wang et al., "Reactive Power Optimization of Wind Farm Considering Reactive Power Regulation Capacity of Wind Generators," IEEE Xplore, https://ieeexplore.ieee.org/stamp/stamp.jsp?tp=&arnumber=8881439.

[45] C. Moldoveanu et al., "Requirements of a real time monitoring and analysis system of power losses in electrical transmission and distribution systems," IEEE Xplore, https://ieeexplore.ieee.org/stamp/stamp.jsp?tp=&arnumber=8759792.

[46] L. Ni et al., "A Review of Line Loss Analysis of the Low-Voltage Distribution System," IEEE Xplore, https://ieeexplore.ieee.org/stamp/stamp.jsp?tp=&arnumber=8843146.

[47] A. P. Gupta, A. Mohapatra, and S. N. Singh, "Apparent Power Loss Based Equivalent Model of Wind Farm Collector System," IEEE Xplore, https://ieeexplore.ieee.org/stamp/stamp.jsp?tp=&arnumber=8771713.

[48] F. Xue, X.-F. Song, K. Chang, T.-C. Xu, F. Wu, and Y.-Q. Jin, "Equivalent modeling of DFIG based wind farm using equivalent maximum power curve," in Proc. 2013 IEEE PES General Meeting, July 2013, pp. 1–5.

[49] L. Liang et al., "The Influence on Power System Loss from Large Scale Wind Farm Integration," IEEE Xplore, https://ieeexplore.ieee.org/stamp/stamp.jsp?tp=&arnumber=8610784.

[50] B. Chen et al., "Theoretical Line Loss Calculation of Distribution Network Based on the Integrated electricity and line loss management system ," IEEE Xplore, https://ieeexplore.ieee.org/stamp/stamp.jsp?tp=&arnumber=8592309.

[51] Y. C. Chen, P. Dong, and Z. D. Wu, "Analysis of Power Flow in Wind Farm with Matpower," IEEE Xplore, https://ieeexplore.ieee.org/stamp/stamp.jsp?tp=&arnumber=8277777.

[52] D. Sun et al., "Optimal Reactive Power Flow Considering Generator Voltage Regulation Characteristics ," IEEE Xplore, https://ieeexplore.ieee.org/stamp/stamp.jsp?tp=&arnumber=8216068.

[53] S. C. Vegunta, M. J. Barlow, and S. Stapleton, "Reactive Power Compensation Solutions and Reactive Power Source Priority Impact on Wind Farm Losses ," IEEE Xplore, https://ieeexplore.ieee.org/stamp/stamp.jsp?tp=&arnumber=7979753.

[54] F. M. F. Flaih, L. Xiangning, S. M. Dawoud, and M. A. Mohammed, "Distribution System Reconfiguration for Power Loss Minimization and Voltage Profile Improvement Using Modified Particle Swarm Optimization ," IEEE Xplore, https://ieeexplore.ieee.org/stamp/stamp.jsp?tp=&arnumber=7779482.

[55] P. R. Babu and S. B, "Operation and Control of Electrical Distribution System with Extra Voltage to minimize the Losses ," IEEE Xplore, https://ieeexplore.ieee.org/stamp/stamp.jsp?tp=&arnumber=6527643.

[56] L. MIHET-POPA and V. GROZA, "Annual Wind and Energy Loss Distribution for Two Variable Speed Wind Turbine Concepts of 3 MW," IEEE Xplore, https://ieeexplore.ieee.org/stamp/stamp.jsp?tp=&arnumber=5944340.

[57] N. Inaba et al., "A consideration on loss characteristics and annual capacity factor of offshore wind farm," IEEE Xplore, https://ieeexplore.ieee.org/stamp/stamp.jsp?tp=&arnumber=6350160.

[58] "FERC transmission reform paves way for adding new energy resources to grid," Federal Energy Regulatory Commission, https://www.ferc.gov/news-events/news/ferc-transmission-reform-paves-way-adding-new-energy-resources-grid.

[59] "Electric Vehicle Battery Pack costs in 2022 are nearly 90% lower than in 2008, according to DOE estimates," Energy.gov, https://www.energy.gov/eere/vehicles/articles/fotw-1272-january-9-2023-electric-vehicle-battery-pack-costs-2022-are-nearly.

[60] "2022 Odessa disturbance," NERC, https://www.nerc.com/comm/RSTC_Reliability_Guidelines/NERC_2022_Odessa_Disturbance_Report%20(1).pdf.

[61] Grid connection requests grow by 40% in 2022 as clean energy surges, despite backlogs and uncertainty, https://emp.lbl.gov/news/grid-connection-requests-grow-40-2022.

[62] Marathon Electric Generators, https://www.marathongenerators.com/generators/docs/manuals/SB317.pdf.

[63] J. Keller and B. Kroposki, Understanding Fault Characteristics of Inverter-Based Distributed Energy Resources, https://www.nrel.gov/docs/fy10osti/46698.pdf.

[64] "How Do Distributed Wind Energy Systems Work?," Office of Energy Efficiency & Renewable Energy, https://www.energy.gov/eere/wind/how-do-distributed-wind-energy-systems-work-text-version.

[65] "Current Protocols - Nodal," Electric Reliability Council of Texas, https://www.ercot.com/mktrules/nprotocols/current.

[66] The Power Flow Equations, https://home.engineering.iastate.edu/~jdm/ee458_2011/PowerFlowEquations.pdf.

[67] Wind Energy Market Value | Electricity Markets and Policy Group, https://emp.lbl.gov/wind-energy-market-value.